Trinity University
Digital Commons @ Trinity

Geosciences Faculty Research | Geosciences Department

8-2022

The Role of Fracture Branching in the Evolution of Fracture Networks: An Outcrop Study of the Jurassic Navajo Sandstone, Southern Utah

Benjamin E. Surpless
Trinity University, bsurples@trinity.edu

Caroline McKeighan

Follow this and additional works at: https://digitalcommons.trinity.edu/geo_faculty

 Part of the Earth Sciences Commons

Repository Citation

Surpless, B., & McKeighan, C. (2022). The role of fracture branching in the evolution of fracture networks: An outcrop study of the Jurassic Navajo Sandstone, southern Utah. *Journal of Structural Geology, 161*, Article 104664. http://doi.org/10.1016/j.jsg.2022.104664

This Post-Print is brought to you for free and open access by the Geosciences Department at Digital Commons @ Trinity. It has been accepted for inclusion in Geosciences Faculty Research by an authorized administrator of Digital Commons @ Trinity. For more information, please contact jcostanz@trinity.edu.

Title:

The role of fracture branching in the evolution of fracture networks: an outcrop study of the Jurassic Navajo sandstone, southern Utah

Authors:

Surpless, Benjamin*, and McKeighan, Caroline**

*_Corresponding author_: (email: bsurples@trinity.edu) Trinity University, 1 Trinity Place, San Antonio, TX, 78209

**Bureau of Economic Geology, Jackson School of Geosciences, University of Texas, Austin, TX, 78712

Keywords:

Fracture branching, fracture network, fluid flow, earthquakes, damage zone

ABSTRACT

Fractures strongly influence the permeability of geologic formations, and because most fractures in the subsurface are below the resolution of geophysical methods, predicting the spatial evolution of fracture networks is important for groundwater resources, oil and gas production, and geothermal energy. Previous researchers have established that variations in lithologic mechanical properties influence the propagation of joints and fractures in layered rocks under stable stress conditions, but few studies have addressed how instabilities in local stress fields, in conjunction with variations in rock mechanical properties, lead to fracture branching.

We investigate NE-striking fractures in the footwall of the west-dipping Sevier fault in Utah, USA, where canyons expose the sub-horizontal Jurassic Navajo Sandstone. We analyzed field data, petrographic data, and unmanned-aerial-vehicle (UAV) imagery to document the fracture network. We also used structure-from-motion (SfM) software to build a 3D virtual outcrop model, measuring 100 m high and 260 m wide, to aid our analysis of fracture network geometry, intensity, and spacing variations.

Data reveal an up-section increase in fracture intensity and decrease in spacing regularity partly accommodated by upward fracture branching. We suggest that branching was initiated by a combination of changes in mechanical behavior within cross-bed sets and twist hackle propagation associated with mixed mode fracture systems. These tree-like fracture geometries may be associated with high-velocity, earthquake-related fracture propagation events. Fracture branching strongly influences permeability and should be considered by researchers investigating fracture development in subsurface systems.

1. Introduction

Fracture networks strongly influence the permeability of geologic formations, and because these features are below the resolution of conventional geophysical methods (e.g., Cooke, 1997), predicting the spatial distribution of fractures based on the dynamic evolution of those networks is important for those involved with oil and gas exploration and production (e.g., Aydin, 2000; Knipe et al., 1998; Nelson, 2001; Narr et al., 2006), rates of groundwater flow (e.g., Rowley, 1998), and localization of ore mineralization (e.g., DeWitt et al., 1986). Previous researchers have established that fracture initiation and propagation are strongly affected by structural position relative to a fold or fault and the variation in mechanical properties within a geologic unit (e.g., Evans and Dunne, 1991; Ferrill and Dunne, 1989; Hickman et al., 2009; Smart et al., 2012). Fracture network development is also affected by variations in the strength of coupling between beds, even at relatively low cumulative strains (e.g., Cooke and Pollard, 1997; Smart et al., 2009; Surpless and Wigginton, 2020).

However, with the exception of studies focused on induced hydraulic fracturing in shales (e.g., Chau et al., 2016; Rabimi-Aghdam et al., 2019), few studies have addressed the role of fracture branching in increasing fracture intensity within naturally fractured rock. Physical experiments and numerical modeling of both stable and unstable fracture propagation reveal that a propagating fracture will split into two or more fractures when it is more energetically favorable than continued propagation of a single fracture (e.g., Ramulu and Kobayashi, 1984; 1985; Shukla et al., 1990; Sharon and Fineberg, 1996; Zhou et al., 2018), and Fineberg and Bouchbinder (2015) suggest that the tip process zone may provide a feedback to crack propagation that results in the unstable behavior that causes fracture branching.

Many researchers have suggested that mode I fracture branching is velocity dependent, with branching associated with unstable propagation only occurring at a critical propagation velocity at about 0.3-0.4 the Rayleigh wave velocity (v_{cr}) of the material (e.g., Freund, 1990; Kulander and Dean, 1995; Marder and Fineberg, 1996; Rosakis and Ravichandrand, 2000; Sagy et al., 2001; Bhat et al., 2012; Shulz, 2019). Therefore, the rarity of branching observed in tectonic joint sets has been used to infer that the velocity of tectonic fracture propagation is both stable (e.g., Engelder, 2007) and slow, with crack propagation rates of up to cm/s only possible in cases of large local driving stresses (e.g., Segall and Pollard, 1983; Savalli and Engelder, 2005). However, Sagy et al. (2001) used a combination of field data and experimental results to suggest that branching observed in some field exposures can indicate dynamic, high-velocity fracture propagation in rocks affected by regional extension.

Braunagel and Griffith (2022) cautioned that many of the experiments used to constrain the critical propagation velocity for branching were performed upon engineered materials, so extending those results to natural geologic materials might not be appropriate. Other researchers have suggested that the propagation instabilities required for fracture branching at the fracture tip may occur at slower propagation velocities (Ravi-Chandar and Knauss, 1984a,1984b; Fineberg and Bouchbinder, 2015, *and refs. therein*), with mixed mode fractures providing an asymmetry in the tip zone that may promote branching at lower velocities than a tensile fracture (Fineberg and Bouchbinder, 2015, *and refs. therein*). Importantly, the stress-intensity factor and the remote stress field also affect fracture-branching from a propagating tensile crack tip (e.g., Shukla et al., 1990), and weak interfaces between layers impact not only the direction of propagation but may promote the initiation of fracture branching (e.g., Xu et al., 2003; Chalivendra and Rosakis, 2008; Sundaram and Tippur, 2016).

To investigate natural fracture branching in geologic materials, we use field data to document and analyze the distribution and orientation of fractures in the footwall of the NNE-striking, west-dipping Sevier fault at a site in south-central Utah (Fig. 1). There, a canyon at high angles to fault strike has eroded into the well-studied Jurassic Navajo sandstone (Fig. 2; e.g., Cooke, 1997; Rogers et al., 2004; Fossen et al., 2011). This canyon provides spectacular vertical and horizontal exposure both parallel and perpendicular to fault strike, permitting us to document the fracture network, through approximately 100 meters of the stratigraphy. Because most of the fracture network is inaccessible, we use unmanned-aerial-vehicle (UAV) imagery and structure-from-motion (SfM) technology to build a sub-decimeter-resolution 3D, georeferenced virtual model of a 100-m-high, 260-m-wide outcrop.

Our data show an up-section increase in fracture intensity and a decrease in the regularity of fracture spacing within the massive Jurassic Navajo sandstone, with exponential increases in intensity associated with upward fracture branching. We provide mechanical explanations for upward fracture branching and associated changes in fracture network characteristics. These explanations have implications for fluid flow in aquifer systems (e.g., Rowley, 1998), for localizations of ore mineralization (e.g., DeWitt et al., 1986), and for sandstone reservoir systems, where massive marine and terrestrial siliciclastic units in the subsurface have been and will continue to be some of the most productive hydrocarbon reservoirs worldwide (e.g., Morse, 1994, *and refs. therein*; McKie et al., 2010; Al-Masrahy et al., 2012).

2. Background

2.1 The Sevier Fault, the Orderville geometric bend, and Red Hollow Canyon

In southcentral Utah, three major, right-stepping, steeply west-dipping normal faults accommodate strain across the transition zone between the raised and relatively stable

Colorado Plateau to the east and the highly-extended Basin and Range province to the west (Fig. 1). These faults, from west to east, are the Hurricane fault, the Sevier-Toroweap fault, and the Paunsaugunt fault (e.g., Stewart and Taylor, 1996; Davis, 1999). The Sevier fault has accommodated extension across the transition zone since the Miocene (e.g., Reber et al., 2001; Lund et al., 2008), and previous researchers have suggested the fault is capable of producing significant earthquakes (Anderson and Rowley, 1987; Doelling and Davis, 1989; Anderson and Christenson, 1989; Lund et al., 2008).

Our study area is within the complex Orderville geometric bend, near Orderville, Utah, where three segments of the Sevier fault, including the Mt. Carmel, Orderville, and Spencer Bench segments, accommodate extension (Fig. 2) (Doelling and Davis, 1989; Schiefelbein, 2002; Doelling, 2008). At this latitude, the Sevier fault zone accommodates approximately 760 m normal fault throw (Scheifelbein, 2002). We investigate fractures exposed in the walls of Red Hollow Canyon in the footwall of the Spencer Bench segment (see "VOM model area" in Fig. 2).

2.2 Exposed Jurassic Navajo Sandstone stratigraphy

The oldest sedimentary rock in Red Hollow Canyon is the cliff-forming Lower Jurassic Navajo Sandstone, a unit that varies in thickness across southcentral Utah from 400 m to 670 m (Doelling, 2008). Porosities for the well-sorted and well-rounded eolian quartz sandstone are typically between 20-25% across the Colorado Plateau (Fossen et al., 2011). The Red Hollow Canyon exposes the uppermost 200 meters of the sandstone, which crops out as stacked, cross-bedded units without any massive, planar beds recognized at other localities (Doelling, 2008). The Navajo sandstone consists of a lower, red, oxidized unit and an upper, light-gray, bleached unit (e.g., Peterson and Pipiringos, 1979; Sargent and Philpott, 1987; Doelling and Davis, 1989), both well-exposed at Red Hollow Canyon. At other localities, it has been demonstrated that this

color change has no clear relationship with Navajo Sandstone bedding features (Peterson and Pipiringos, 1979).

Dune cross-strata like those in the Navajo Sandstone are built from sloping grain-flow layers created by sand avalanching down the lee slip face of a migrating dune (e.g., Nickling et al., 2002). Sorting occurs during grain flow, resulting in the coarsest and best-sorted sand grains in the basal portions of each dune form, with poorer sorting up dip from the basal surfaces. Thinner, fine -grained grainfall layers commonly separate grain flow layer crossbeds, resulting in differential weathering that makes these layers easy to document in the field. However, these grainfall layers are not always preserved in outcrop.

The mechanical stratigraphy of the Navajo sandstone depends on dune layer thicknesses and variations in inter-dune layer thicknesses and strengths (Cooke, 1997). Cooke (1997) considered the formation to be a stack of relatively homogeneous layers (crossbed sets) with different thicknesses and variation in the character of inter-dune-layer contacts. The basal deposits that commonly separate the dune layers are much more variable in nature than the dune layers, with strengths that vary according to the level of cementation and thicknesses that change laterally along the horizon (Cooke, 1997).

2.3 Fault damage zones and fracture orientation

The initiation, propagation, and increase in total slip along a fault and the interaction between propagating faults impact fracture formation in rock volumes adjacent to fault segments (e.g., Flodin and Aydin, 2004a; 2004b; Kim et al., 2004; Choi et al., 2016; Peacock et al., 2017). Researchers have classified damage zones based on their location within a fault zone complex, including: tip damage zones, which form in the volume of rock proximal to the fault tip (e.g., Cowie and Scholz, 1992; Reches and Lockner, 1994; Vermilye and Scholz, 1998; Kim et

al., 2004; Choi et al., 2016); wall damage zones, which form in the wall rocks of a fault as slip along the fault increases (e.g., McGrath and Davison, 1995; Kim et al., 2004; Choi et al., 2016); and linking damage zones (e.g., Zhang et al., 1991; Kim et al., 2003; 2004; Choi et al., 2016). In addition, damage zones may form due to slip along geometric irregularities in the fault plane as well as due to rupture propagation along pre-existing fault surfaces (e.g., Mitchell and Faulkner, 2009). As fractures form in these damage zones, lithology, bed thickness, mechanical stratigraphy, pre-existing fractures, and the presence or absence of inter-layer slip impact their development (e.g., Price, 1959; Couples and Lewis, 1998; Cooke and Underwood, 2001; Nelson, 2001; Bergbauer and Pollard, 2004; Smart et al., 2009; McGinnis et al., 2015; Surpless and Wigginton, 2020).

As normal fault segments propagate, the stress field adjacent to isolated or interacting faults is perturbed relative to the remote tectonic stress field, resulting in a range of possible fracture orientations and patterns (e.g., Price and Cosgrove, 1990; Rives et al., 1992; Kattenhorn et al., 2000). Based on numerical modeling and field data, Kattenhorn et al. (2000) showed that fractures can grow at high angles to a normal fault plane near the lateral tips of normal faults, and they also demonstrated that a perturbed stress field extends furthest from fault segments proximal the lateral fault tipline and within relay zones between normal fault segments. The location of the VOM outcrop in the footwall of and near the southern tip of the Spencer Bench segment (Fig. 2), likely experienced a perturbed stress field during slip along that fault segment.

2.4 Fracture Branching in Geologic Materials

Although there is no field-based method to deduce the propagation velocity of a fracture (e.g., Engelder and Fischer, 1996), Sagy et al. (2001) proposed field criteria for dynamic

fracturing of rock layers, leveraging both field and experimental data. They suggested that the geometry of branched fractures in the field and in dynamic (high crack propagation velocity) experiments displayed closely spaced fractures related by "tree-like" branching geometries, with secondary fractures branching from a main fracture and smaller fractures branching from the secondary fractures, with further subsidiary branching also possible. Sagy et al. (2001) also showed that within a given "tree-like" fracture complex, conjugate sets of fractures developed, with angles that remained relatively constant throughout the structure. Physical and numerical dynamic fracturing experiments support a preferred branching angle of 30° from the initial fracture (e.g., Isida and Noguchi, 1992; Abraham et al., 1994; Sharon and Fineberg, 1996), which is roughly consistent with the results of Sagy et al. (2001).

Initially, these results appear to violate theoretical models of the maximum limits of joint density in rock layers based on the stress shadow concept (e.g., Gross et al., 1995; Bia and Pollard, 2000; Olson, 2004). However, Sagy et al. (2001) proposed that dynamic fracturing at high strain rates (e.g., 4×10^{-3} s^{-1}) should not be considered within that theoretical framework, suggesting instead that dynamic fracturing be considered a new mechanism for the development of high fracture densities. Sharon and Fineberg (1996) suggested that it is easier for a rock to dissipate energy by initiating branches rather than by increasing propagation velocity along a simple tensile fracture, and Griffith et al. (2009) confirmed this experimentally, showing that that the creation of new fracture surface area reduced the energy available for propagation. In their field-based investigation, Sagy et al. (2001) demonstrated that branching from an initial fracture results in a total complex fracture area that is up to 17 times that of a simple planar fracture. However, over time, these branched complexes may fill in unfractured regions across the same layer (Sagy et al., 2001), resulting in a final spacing of tree-like fracture

complexes that is comparable to planar fractures filling in the width of a layer, as governed by classic stress-shadow mechanics. Importantly, these fracture branching geometries, likely created by dynamic fracturing associated with past earthquakes, might provide a way to recognize past seismic events in the rock itself (Sagy et al., 2001; Melosh et al., 2014).

3. Methods

3.1 Field methods and thin section petrography

We collected structural data from the Red Hollow Canyon study area using an integrated base map that included digital orthophotos (1-m resolution), and USGS digital elevation models (10-m resolution) downloaded from the USGS National Map in 2016. We measured structural data using standard structural mapping techniques and logged position data using a Trimble Geo XH handheld global positioning system receiver (30 cm accuracy). We compiled all data with a combination of an integrated GIS database and digital maps. We augmented field descriptions and sketches with annotated field photographs of important structural features. We also collected rock samples from different stratigraphic levels within the Jurassic Navajo Sandstone and documented microfractures, textural features, and cementation based on thin section analysis of those samples using a standard petrographic microscope.

3.2 Unmanned aerial vehicle (UAV) surveys and structure-from-motion (SfM) model construction

We executed a series of horizontal UAV flight paths to capture high-resolution video from inaccessible canyon walls and cliff faces across Red Hollow Canyon exposures of the Jurassic Navajo Sandstone. These images permitted us to build a spatially-accurate (0.2-m accuracy; Harrington et al., 2017), georeferenced SfM model of inaccessible rock exposures using *Agisoft Metashape Professional*, following the model-building workflow displayed in Appendix A. Feature-matching algorithms analyze visual data collected from different

perspectives to produce accurate, high-resolution, three-dimensional SfM models (e.g., Lowe, 2004; Johnson et al., 2014). Geologists have used the method to produce high-resolution landscape models in a range of settings (e.g., Westoby et al., 2012; Fonstad et al., 2013; Corradetti et al., 2018). We refer to the completed, georeferenced models as virtual outcrop models (VOMs) for the remainder of this paper.

3.3 Field-based and VOM-based Fracture Mapping

We use the term fracture to represent shear fractures, opening-mode joints, and mixed-mode fractures (with both fracture-perpendicular opening and fracture-parallel shear kinematics). Because we present data gathered from UAV imagery, we do not address fracture-fill characteristics or fracture aperture data. We focused on the best-exposed and most continuous fracture networks on a cliff-face in the footwall of the Spencer Bench segment, where more than a 100 m thickness of the Navajo Sandstone is exposed across approximately 260 meters in map view. This stratigraphic section extends from ground level up to a sharp topographic break within the Navajo Sandstone, where a shallow, poorly-exposed slope prevents us from documenting fracture characteristics. We limited our analysis to fractures longer than 3 meters. For linear scanline analysis of sub-vertical fractures based on direct field observations, we documented the horizontal position of each fracture in a set (sub-parallel fractures with a total strike dispersion of less than 20°) measured perpendicular to fracture orientation. We calculated fracture intensity as the number of sub-vertical fractures per meter along each scanline (e.g., Underwood et al., 2003).

For fracture analysis of our VOM, we used the *Polyline* tool in *AgiSoft Metashape Professional* (*Agisoft*) to trace fractures. The software automatically snaps these lines to the VOM surface. We used our VOM in combination with field observations to address: 1) changes

in fracture intensity with stratigraphic position; and 2) fracture branching geometries. We used *Agisoft* to build an orthomosaic oriented perpendicular to the dominant fracture strike in order to document fracture intensity. We used the orthomosaic to set up scanlines perpendicular to the fractures, keeping each scanline at a consistent position relative to the sub-horizontal bedding. We constructed scanlines at 8 different stratigraphic positions, spaced at 10-m intervals. We estimate that Scanline 1 is approximately 20 meters above our field-based scanline.

We calculated scanline-scale fracture intensity values based on both field data and VOM data by dividing the number of fractures by scanline length. We calculated local fracture intensity by first calculating the average of the spacing between each fracture and its two nearest neighbors and then taking the 5-fracture rolling average of those calculated values to smooth local increases in fracture spacing related to 3 closely-spaced fractures. We then took the inverse of that value to get fracture intensity (from meters/fracture to fractures/m).

We quantified the regularity of fracture spacing using the coefficient of variation, C_v, defined as $C_v = \sigma/\mu$, where σ is the standard deviation of the inter-fracture spacing population and where μ is the mean of the same population (e.g. Gillespie et al., 1999; Hooker et al., 2018; Surpless and Wigginton, 2020). If all fractures on a scanline have identical inter-fracture spacings, the C_v value will be zero; as fracture spacing becomes more irregular, the C_v value increases. At a C_v value of 1, spacing is consistent with a randomly distributed fracture population. C_v must exceed 1 by an amount that depends on the total number of fractures in a population for that population to exhibit non-random clustering (e.g., Hooker et al., 2018).

4. Data and Results

We investigated well-exposed fractures through a 100-meter-thick section with a base approximately 200 m below the top of the ~620-m thick (e.g., Doelling, 2008), sub-horizontal Jurassic Navajo Sandstone. We focus on vertical changes in fracture character, intensity, and geometry, using our analysis to address the evolution of fracture systems in massive sandstone units.

4.1 Characteristics of the Jurassic Navajo Sandstone

The Navajo sandstone's most prominent feature is its spectacular crossbedding and crossbed sets, up to 20 m thick in the study area (Fig. 3A). Individual crossbeds and inter-dune bedding range in thickness from the mm- to cm-scale near the base of crossbed sets (Fig. 3B), with most crossbeds in the interior of each set displaying tabular forms that are 5-15 cm thick. Crossbeds dip shallowly (<20°) to the south across the study area (Fig. 3A). The sandstone displays a red oxidized zone in the lower exposed section and white/gray bleached zone near the top of the unit. In general, the contact between bleached and oxidized zone is well-defined, but at some locations the transition is gradual or alternates between oxidized and bleached horizons. At the study site, there is a break in slope from the bleached section (~36° slope) to the shallower red oxidized section (~23° degree slope), suggesting a difference in relative resistance to erosion. Although the boundary between the bleached and oxidized zones sometimes coincides with the contact between crossbed sets, primary structures within the Navajo sandstone do not appear to strongly influence the boundary, consistent with the work of previous researchers (Surdam et al., 1993; Nielsen et al., 2009), who found no strong stratigraphic control on the transition between these zones.

Thin section analysis of samples from all exposed stratigraphic levels of the Navajo Sandstone reveals grain size that ranges from medium to very-fine sand with sorting that

ranges from well-sorted to moderately-sorted. As expected for an aeolian sandstone, all samples are quartz rich (>90%) with planar or point grain contacts, and samples from the oxidized zone contain iron oxide staining and sometimes reveal iron oxide cement, while cements in the bleached samples only rarely display visible iron oxide content. Based on visual inspection, we did not discern obvious differences in the concentration of cements (relative to porosity) between the oxidized and bleached samples. Micro-fractures less than 3 mm are present in most samples, affecting grains and cements, but these fractures display no preferred orientation, consistent with the findings of Hankla and Judge (2019).

4.2 Fracturing in the Navajo Sandstone

Across the study area, most fractures in the Jurassic Navajo sandstone strike NNE to NE and dip steeply (>75 degrees to vertical) to the WNW. However, at the primary investigation site, in the footwall of the Spencer Bench segment, fractures strike ~N50°E, which is more northeasterly than the adjacent NNE-striking fault segment or other fractures in the hanging wall of the Spencer Bench segment (see joint symbols in Fig. 2). This observed deviation of fractures from orientations subparallel to the fault may be related to deviation of the principal stresses caused by alternation of zones of strong and weak cross-fault contact parallel to fault strike (e.g., Petit et al., 2000). Using this model, the Spencer Bench segment adjacent to the study site would have acted as a weak fault section that was served as a stress barrier between the footwall and hanging wall during fracture initiation and propagation. However, the orientation of joints in the footwall might also be explained by a perturbed stress field adjacent to the tip of the Spencer Bench segment as it propagated to the south (e.g., Kattenhorn et al., 2000; Maniatis and Hampel, 2008) or by stress-field deviation associated with interacting normal fault segments (e.g., Kattenhorn et al., 2000) (Fig. 2).

At ground level, fractures are sometimes filled with cement and in other cases exhibit opening-mode separations without cement. Importantly, we could identify and measure fractures that displayed only mm-scale expression in outcrop; we note this here because fractures with little outcrop expression would not be visible in UAV-based imagery (this has implications for quantitative comparison of ground-based vs. UAV-based data). In some cases in Red Hollow Canyon, to the west of the VOM model area, WNW-dipping fractures at lower dip angles (< 75 degrees) exhibit down-to-the-WNW displacements of up to 1 m (Fig 4A), but for most fractures, we did not observe shear displacement. Although deformation bands are common in the Navajo sandstone at other localities in Utah (e.g., Fossen et al., 2011), they are rarely observed in Red Hollow Canyon outcrops, so we do not address them here.

Ground-based observations of fracturing across Red Hollow Canyon reveal variations in both the intensity and character of fracturing. At ground level near the investigation site, fractures are commonly widely spaced (>3 m between fractures), while higher in the exposed stratigraphy, fracture spacing decreases (Figs. 4B and 4C). Near the top of the exposure shown in Figure 4B, there appears to be an abrupt change in fracture intensity from relatively planar, well-defined, widely-spaced fractures to an upper zone with higher fracture intensity. Most prominent in this upper zone are two fracture corridors (as defined by Questiaux et al., 2010) with much more intense fracturing (Fig. 4C) than the rocks to the northwest or southeast. However, our field-based, ground-level observations of these up-section changes in fracture intensity are qualitative; we were not able to determine the geometric relationship between fractures at the bottom of Figure 4B relative to those at the top of the image.

Although the focus of this investigation is primarily upon fractures longer than 3 meters, shorter fractures reveal the role that crossbed contacts and crossbed-set contacts can play in

the initiation and arrest of vertical fractures. At many localities across the field area, short fractures in a given set are commonly arrested at a specific crossbed contact or crossbed set contact (Fig. 4D). In other cases, some fractures within a set terminate at a contact while others propagate across the contact but change orientation, refract, or may intersect fractures propagating from the other side of the contact (Fig. 4D). These data suggest that at low strains, even small changes in elastic moduli, either within cross bed sets or from one cross bed set to another, can affect fracture propagation trajectory and/or termination. Alternatively, close inspection of these fractures reveals that most fractures are perpendicular to the orientation of crossbeds, not the crossbed set contacts (Fig. 4D), suggesting that the crossbed contacts may be weak (low-traction) boundaries that control local principal stress orientations (e.g., Cooke, 1997; Cooke et al., 2000). Thus, changes in bed orientations above and below a cross-bed set contact might lead to the change in fracture orientations across these contacts (instead of a change in mechanical properties of the sandstone across the contact).

We also observed fracture branching geometries across a range of scales. In most cases, curved splay fractures appear to have initiated from a planar fracture (Fig. 5). In all cases, these systems exhibit an upward-branching geometry, with splay fractures that display a range of lengths above the branching point; at some localities, all splay fractures are vertically continuous above the branching point, but at most sites, some splay fractures terminate a short distance above their initiation point while other splay fractures are vertically continuous above their branching location. In Figure 5B, a planar fracture without evidence for shear displays a series of curved splay fractures near the top of the outcrop that eventually become subparallel to the main fracture, but several of these splay fractures terminate a short distance from their branching point. Interestingly, six fractures to the east of the main fracture appear to initiate at

a crossbed contact without an observable physical connection with the vertically-continuous main fracture, but their geometries are consistent with the splays to the west, adjacent to the lens cap (Figs. 5A and 5B). This relationship suggests that bed contacts may play an important role in the initiation of splays adjacent to planar fractures.

We did not observe structures on fracture planes that permitted us to determine propagation direction (e.g., plumose or hackle features), but our ability to observe these features is hindered both by the degree of surficial weathering and because we cannot directly observe fracture planes (i.e., most branching was documented based upon UAV-based imagery). We also did not observe Wallner lines, features that ornament fractures that have propagated at rates similar to a rock's sonic velocity (Kulander and Dean, 1995; Schulz, 2019). However, Wallner lines are rounded, ripple-like curves preserved within the mirror zone of fractures in amorphous or fine-grained materials (Wallner, 1939; Field, 1971), so it is unlikely that the medium-grained Navajo sandstone would preserve them in field exposures.

In Figure 5C (from UAV-based imagery of the VOM model area), most splay fractures remain present to the top of the exposure, with many splay fractures curving toward orientations subparallel to the main fracture. Some exposed fracture branching geometries are similar to horsetail splays or synthetic branch fractures, suggesting a possible mixed-mode (mode I/II or I/III) origin (e.g., Petit and Barquins, 1988; Kim et al., 2004; Kim and Sanderson, 2006). Interestingly, several documented branching systems shown in Figure 5C have geometries centered within the same crossbed set, and in most cases, the branching geometries are similar, with the main fracture sub-vertical and the branching splay fractures to the southeast of the main fault dipping toward the northwest.

As we collected data for scanline analysis based on direct observations in the field), we also collected fracture orientations (equal-area stereonet in Fig. 6) within the bounds of the VOM area (Fig. 2). These fractures display strike values rotated ~30° to the NE relative to the Spencer Bench fault segment and display steep NW dips between 68 degrees and vertical (Fig. 6). The average dip of these fractures is 84° NW with 5.4° standard deviation. Because visibility was limited within the steep-walled inner canyon, we cannot directly correlate field-based observation of fractures with fractures documented on the VOM.

4.3 Fracture Geometry

We used two "bird's-eye view" flights along the VOM Model area (Fig. 2) to capture imagery for the VOM displayed in Figure 6. A map view of the georeferenced model, shown with all fractures documented (yellow lines in Fig. 6), reveals the dominant northeast strike of fractures across the scanline. These VOM-based fracture orientations are consistent with attitudes of ground-based scanline fractures (Fig. 6). As described earlier, the strike of this fracture set is at an angle of ~30° clockwise relative to the strike of the Spencer Bench fault segment, and the scanline orientation, trending N30°W, is perpendicular to fracture strike (Fig. 6).

The fracture network displayed in Figure 7 reveals that very few fractures propagate through the entire exposed stratigraphy. However, in many cases, it appears that tips of stratigraphically lower and higher fractures nearly meet, suggesting that either: 1) these apparently separate fractures may be a continuous fracture within the rock volume that terminated laterally very close to the surface; or 2) weathering and erosion of the exposed fracture varies along its length, so that even at high model resolutions, we cannot see a small

segment of what is actually a continuous fracture; or 3) spatially discrete fractures propagated from different initiation points and coincidentally terminated prior to direct connection.

We did not identify any cross-fractures between fractures in the dominant set, and we only rarely documented closely-spaced fractures that affected the propagation paths of the fractures around them. Instead, most un-branched fractures in the network appear to initiate and terminate without visible stress-related interactions with nearby neighbors. We documented fracture branching geometries at 30 locations across the VOM (Fig. 7), with only two branching geometries present in the red, oxidized zone, 6 branching geometries in the transition zone, and all remaining branching geometries (>70%) in the upper, light gray, bleached zone, which coincides with scanlines 6, 7, and 8 (Fig. 7). In addition, we only observed fractures that split into multiple fractures at a higher stratigraphic levels, as opposed to multiple fractures that merged into single fractures at higher stratigraphic levels.

In Figure 8, we display 5 prominent complexly-branched fracture systems with splay fractures that stem from a primary, steeply SE-dipping primary fracture. The average branch angle for these systems ranges from 14° – 20°, with a minimum branch angle of 7° and a maximum branch angle of 39°. In the case of fracture complex 5 (Fig. 8B), we indicate examples of branching at the uppermost levels of the outcrop within that system with the annotation 5* (Fig. 5C). These geometries are remarkably similar to both naturally and experimentally produced twist hackle, which is generated under mixed mode I-III loading of a propagating crack (e.g., Pollard et al., 1982; Cooke and Pollard, 1996). Pollard et al. (1982) demonstrated that growth of these splays will twist about axes parallel to the propagation direction of the "parent" crack that eventually re-aligns the splay plane into an orientation consistent with the remote principle stress plane. This mixed-mode explanation for fracture

branching would be consistent with fractures that strike ~30° from the strike of normal faults and other opening mode fractures across the study area near the southern tip of the Spencer Bench segment (Fig. 2).

Although at a different scale than the complex fractures described by Sagy et al. (2001), the geometries here are remarkably similar to the type example given in that study (Fig. 8C). The average branching angle in the Sagy et al. (2001) study was approximately 30°, but our fracture splay angles fall within the variability documented in that study. In one fracture complex included in that study, there are 8 generations of branching (e.g., an initial splay fracture from the primary stem is the second generation, and a splay fracture from that secondary splay would be a third generation). In contrast, most fracture branches documented in this study stem from the primary fracture, with only 4 generations of branching present in our examples (with most displaying just 2 generations).

However, we suggest that the different scales of observation and types of lithology fractured may impact the number of branching generations observed in these complex fracture systems. Sagy et al. (2001) documented their fracture network using standard field observations of a single, 3.3m-thick layer of fine-grained dolomite, while our observations were based on UAV-based imagery of a massive, medium grained sandstone. Our scale of observation does not permit us to resolve mm-scale fractures across the outcrop, which limits our ability to document the higher generations of fracture branching on a scale similar to that documented in Sagy et al. (2001) (Fig. 8C). In addition, because lithologic properties affect fracture network development, we would expect differences in branched fracture complexes under identical loading conditions.

4.4 Fracture Intensity

Scanline data reveal lateral variability in fracture spacing across both field and VOM-derived scanlines 1-8 (Fig. 9; Data Repository Item). On the field scanline, there are two zones of higher fracture intensities (F.I.) at ~50-60m and at ~125-140 m (Fig. 9), but the positions of those fractures do not correlate up-section with similar zones in Scanline 1. However, the position of zones of elevated F.I. (as identified by relative and absolute maxima on the normalized, smoothed fracture intensity graphs) on stratigraphically lower VOM-based scanlines commonly correlate with positions of elevated F.I. in suprajacent scanlines. For instance, the positions of two zones of high F.I. along Scanline 1 (at ~70m and ~170m) correlate with high F.I. zones in Scanline 2, Scanline 3, and in all scanlines up section (Fig. 9).

Average F.I. increases up section, from 0.165 m^{-1} for Scanline 1 to 0.700 m^{-1} for Scanline 8, while the field scanline at the base displays a F.I. of 0.341 m^{-1} (Fig. 9). However, because we can identify fractures at ground level that we would not be able to recognize on VOMs (see *Fracturing in the Navajo sandstone*), we do not directly compare ground-based and VOM-based data. For VOM data, the upward increase in F.I. best follows an exponential function with strong goodness of fit (R^2=0.967) (Fig. 10). The increase in F.I. from scanlines 1 through 5 averages 0.035 m^{-1} per scanline, while the increase from scanlines 5 through 8 averages 0.132 m^{-1}. The change from smaller to larger changes in F.I. with increasing stratigraphic level coincides with the transition from oxidized to bleached Navajo sandstone (Figs. 9 and 10). We note that there is no relationship between fracture intensity values and distance from the Spencer Bench fault segment (Fig. 6).

We use C_v values to assess the regularity of fracture spacing at different stratigraphic levels within the Navajo Sandstone. Our data reveal that fracture spacing is more irregular at higher stratigraphic levels (scanlines 5-8) relative to lower stratigraphic levels (scanlines 1-4)

(Table 1; Fig. 9). Our analysis shows that no statistically significant clustering (C_v at or above the 95% confidence limit required for non-random clustering; Hooker et al., 2018) is present at any level within the stratigraphy (Table 1). However, data from scanlines 5 through 8 display much more irregular fracture spacing (0.08 – 0.18 below the C_v 95% conf. limit) relative to the lower four scanlines (0.29-0.45 below the C_v clustering limit) (Table 1; Fig. 9). Similar to F.I. data, this change in behavior coincides with the change in coloration from the red, oxidized Jurassic Navajo Sandstone to the light gray Navajo Sandstone (Figs. 9 and 10).

5. Discussion

Outcrop studies like ours are commonly used to develop fracture populations in models of subsurface systems (e.g., Becker and Gross, 1996; Wennberg et al., 2007; Barbier et al., 2012; Bisdom et al., 2016), in part because fracture spacing impacts the likelihood of fracture intersection during subsurface drilling (e.g., Narr et al., 1996; Hooker et al., 2018). However, these rocks have been exhumed from depth, so caution must be used when comparing surface and subsurface systems (e.g., McGinnis et al., 2015; Corradetti et al., 2018; Laubach et al., 2019). Nonetheless, our results provide important information about the vertical development of fracture networks within thick sandstone units that would not be accessible in a subsurface system.

Although a multitude of previous studies have provided general rules and scale relations that govern joint and fracture formation (e.g., Ladeira and Price, 1981; Narr and Suppe, 1991; Gross, 1993; Bai and Pollard, 2000; Bonnet et al., 2001; Olson, 2003; Odonne et al., 2007; Laubach et al., 2009; Hooker et al., 2013), in the case of fracture network formation in poorly stratified lithologies with less predictable frictional interfaces, like the Navajo sandstone, these principles are more difficult to apply (e.g., Corradetti et al., 2018). Below, we focus upon: 1)

the possible impact of primary structures and vertical changes in the elastic behavior of the Navajo sandstone upon fracture branching and intensity; 2) a model of twist-hackle mixed-mode fracture propagation that explains complexly branched fracture geometries; 3) an alternative explanation for fracture branching documented in this study; and 4) the role that fracture branching played in the evolution of fracture network characteristics.

5.1 The role of redox reactions, cementation, and primary structures on fracture development

Eolian dune deposits commonly redden soon after deposition and during early diagenesis due to iron oxidation, which forms hematite cements and coatings on detrital grains (e.g., Walker et al., 1978; Turner, 1980; Parry et al., 2004). Bleaching of sandstone is post-depositional, with iron removed by reduction reactions associated with hydrocarbons, hydrogen sulfide, organic acids, methane or other chemical agents (e.g., Dixon et al., 1989; Chan et al., 2000; Beitler et al., 2003; Parry et al., 2004). However, after the mobilization and removal of significant iron oxide from the Navajo Sandstone during bleaching, Nielsen et al. (2009) used compositional and petrographic data to suggest a renewed period of cementation under oxidizing conditions, even where no obvious reddish staining was present.

We suggest that the oxidized and bleached zones within the Navajo Sandstone may correlate with different types and concentrations of cementation, which in turn impact the mechanical properties of the two zones, consistent with the change in topographic slope associated with the two zones at Red Hollow Canyon. With the exception of silica cements, which enhance the strength and stiffness of sandstone (e.g., Dyke and Dobereiner, 1991; Al-Tahini et al., 2006), it has been difficult to experimentally quantify the effects of cementation type on the mechanical properties of sandstones (e.g., Dobereiner, 1984; Nunes, 1989; Dyke and Dobereiner, 1991). Additionally, precipitation or dissolution of cements within host rock or

fractures may alter not only the mechanical properties of the host rock but also the geometries of the fracture patterns that develop (e.g., Laubach et al., 2009; Laubach et al., 2019 *and refs. therein*).

Although our petrographic analysis of oxidized and bleached samples did not show obvious differences in cement concentration, the different cementation histories of the two zones may affect rock behavior (e.g., Laubach et al., 2019). Additionally, because fluid flow through porous media varies based on grain size, with greater flow possible in coarser-grained sandstone, the more complex history of cementation in the bleached zone may have resulted in greater contrasts in cementation between finer- and coarser-grained primary structures (e.g., grainfall vs. grainflow crossbed features). Therefore, upward fracture branching at the study site may have been focused within the bleached Navajo Sandstone due to more abrupt changes in elastic moduli relative to the red, oxidized sandstone.

Previous researchers have investigated fracture and deformation band formation and propagation in the Jurassic Navajo sandstone (e.g., Cooke, 1997; Cooke et al., 2000; Rogers et al., 2004; Fossen et al., 2011), using field data and/or numerical modeling to explain how the massive, cross-bedded sandstone accommodated strain in different geologic settings. Fossen et al. (2011), who focused on compression-related deformation bands, estimated that the top of the Navajo Sandstone was never deeper than about 2 km, with maximum formation burial depth during Laramide time. Based on this estimate and present-day surface exposure of the unit, we suggest faulting and fracturing related to Basin and Range extension took place at less than 1.5 km depth, consistent with the modeling performed by Cooke et al. (2000).

Cooke (1997) and Cooke et al. (2000) used field evidence and numerical modeling of fold development to show that at shallower depths with lower lithostatic stresses, frictional

interfaces at low angles relative to the surface have greater propensity for frictional slip. Although the focus of their work was upon shear failure in fold systems, they also addressed the development of splay cracks associated with fault slip, suggesting that changes in frictional properties along a slip plane can result in stress concentrators that promote splay crack initiation (Cooke, 1997; Cooke et al., 2000). Their focus was upon variations in friction within interdune deposits of the Navajo Sandstone (Cooke, 1997; Cooke et al., 2000), which are relatively planar features at the base of each major crossbed set.

In our study area, the orientations of shorter fracture sets appear to be more strongly impacted by the orientations crossbeds as opposed to interdune deposits Although these shorter fractures commonly terminate at interdune deposits and are oriented at high angles to them, most fractures within a crossbed set appear to be nearly perpendicular to the crossbeds (Fig. 4D), suggesting that contacts between beds may be weak interfaces that locally control principal stress orientations. The initiation of nearly all prominent fracture branching locations at our study site within crossbed sets and not at crossbed set contacts (Figs. 5C and 7) suggests that the relatively low-angle crossbeds may provide mechanical interfaces that set up propagation instabilities required for fracture branching.

5.2 A twist-hackle model for fracture branching

We posit that the location of the study area, in the footwall and near the southern tip of the Spencer Bench segment, experienced a perturbed stress field that evolved over time as fault displacement increased and the lateral tipline of the normal fault propagated southward. The dominant orientation of the studied fractures, rotated ~30° relative to the dominant fracture sets in other areas and relative to the fault itself (Fig. 2), is consistent with a perturbed stress field near the tip of a normal fault (e.g., Kattenhorn et al., 2000). We suggest that a

spatial and temporal variation in the orientation of the stress field proximal to the tip of the Spencer Bench segment led to mixed-mode loading of fractures propagating vertically in the study area, consistent with the work of others investigating similar systems (e.g., Muller and Pollard, 1977; Olsen and Pollard, 1989; Yoenes and Engelder, 1999).

Twist hackle geometries form due to mixed-mode I-III loading, with either continuous or discontinuous propagation of subsidiary fractures from the parent fracture (e.g., Younes and Engelder, 1999). In the study area, we hypothesize that a change in the local stress field led to shear traction on the fracture plane perpendicular to the propagation direction, thus forcing the fracture to partially break down at the tip line and form new fractures consistent with the added Mode III shear component (Fig. 11A). Fracture branching geometries in the study area display smooth curves away from the parent fracture (Fig. 8), suggesting gradual twist hackle formation consistent with the 3D helicoidal pattern of secondary fractures propagation away from the parent tip line (e.g., Pollard et al., 1982; Cooke and Pollard, 1996), as opposed to abrupt twist hackle formation, which is more common as fractures propagate from a bed of one lithology to bed with fundamentally different stiffness (e.g., Younes and Engelder, 1999). In addition, because there are no significant kinks or curves in cross-sectional exposures of parent fractures present across the study outcrop (Figs. 7 and 8), we consider loading to have been primarily mixed-mode I-III with no significant mode II component.

Although the branching events themselves suggest unstable propagation of the parent fracture, the orientations of the parent fractures do not vary significantly with stratigraphic position (Figs. 7 and 8), and splay fractures from the parent fractures appear to have initiated at different stratigraphic levels (Fig. 11B), suggesting multiple twist-hackle initiations during parent fracture vertical propagation. However, because we do not have a 3D view of these

fracture systems, it is possible that 2 or more splays could have initiated synchronously at different locations within the rock volume as the theoretically elliptical (e.g., Katternhorn et al., 2000) parent fracture propagated. We also suggest that propagation instabilities that generated hackle fractures were not enough to cause any significant change in the orientation of the propagating parent fracture. Because the 2D view of hackle fractures only occurs on one side of the parent fracture (Figs. 7, 8, and 11), the non-terminating upward propagating parent fracture may have prevented propagation of hackle fractures across that plane. It may be that fractures generated by a twist hackle mechanism may accommodate enough mode III strain that the vertical propagation of the mode I parent fracture, potentially with a minor shear component of its own, can continue without terminating at the time of twist hackle generation. If true, then the hackle fractures themselves might continue to propagate in concert with the propagating parent fracture.

The propagation of multiple fractures from a single parent fracture in this setting must be more energetically efficient than initiating new, spatially-distinct fractures, but more energy is required to propagate multiple fractures through a rock volume relative to a single fracture. In addition, when multiple fractures form and propagate within a rock body, their stress shadows may overlap and the stress available for propagation may be reduced (e.g., Bai and Pollard, 2000; Olson, 2004). To make up this apparent energy deficit, strain energy associated with one or more earthquakes may have been dissipated within this rock volume, near the tip of the Spencer Bench segment, causing rapid fracture propagation. If so, a range of high fracture propagation velocities is possible, including velocities below, up to, or even greater than the Rayleigh wave velocity (e.g., Ben-Zion, 2001, 2008; Robinson et al., 2006; Bhat et al., 2007; Beroza and Ide, 2011; Fineberg and Bouchbinder, 2015). In addition, the rapid initiation

and vertical propagation of the hackle fractures due to a large input of strain energy might explain why these hackle fractures do not link in cross-sectional view, as might be expected as hackle fractures propagate (e.g., Younes and Engelder, 1999). Finally, Duan and Oglesby (2005) demonstrated that the horizontal component of ground motion during an earthquake is concentrated in the footwall, providing another potential mechanism, in this structural setting, that could introduce fracture propagation instability during such an event.

We suggest that relatively low lithostatic stress at the study site (during Basin and Range extension and at shallow crustal depths) reduced stress normal to shallowly-dipping crossbed layer boundaries, reducing the relative strength of coupling between layers (e.g., Cooke, 1997; Cooke et al., 2000) and enhancing conditions for crack-tip instabilities (e.g., Fineberg and Bouchbinder, 2015) required for twist-hackle formation and branching. Also, nearly all observed branching points were within crossbed sets, suggesting the instabilities that initiated twist-hackle formation/branching were likely associated with parent fracture propagation through crossbedding. The gray upper zone may have a greater variation in degree of cementation associated caused by differences in fluid flow through the coarser grainflow and finer grainfall layers, thus setting up greater mechanical contrasts (relative to the lower, red, oxidized zone) that would more likely lead to fracture propagation instabilities, especially if crack propagation occurs at high velocities (e.g., Sundaram and Tippur, 2016). In addition, twist hackle structures are commonly associated with bedding due to stress-state gradients approaching either a low-traction interface or a bonded interface between materials of different mechanical properties (e.g., Pollard and Aydin, 1988). Finally, our only direct field observation of a branching structure revealed fracture tips apparently localized along a cross-bed or cross-bed set contact without an observable direct contact with the parent fracture

(Figs. 5A and 5B), supporting a model where fractures branching from a parent initiate along beds or contacts.

Finally, although the Jurassic Navajo Sandstone might be considered a massive unit, numerical modeling performed by Olson (2004) revealed stronger mechanical-crack interaction for thicker beds resulting in more intense fracturing in the near tip region, providing an explanation for branching-related high-fracture-intensity zones even where stress-shadow fracture suppression might be expected (e.g., Pollard et al., 1982; Pollard and Segall, 1987; Olson and Pollard, 1991; Rives et al., 1992).

5.3 An alternative explanation for fracture branching

In this article, we have assumed that parent fractures propagated upward and the tree-like geometries documented here were the result of splays initiating from an upward-propagating parent fracture. However, researchers have proposed models where similar up-section increases in fracture intensity are controlled instead by *downward*-propagating fractures. In that model, as fractures propagate downward, the stress shadows surrounding these fractures increase in width due to changes in material properties, terminating the downward propagation of nearby fractures. DeGraaff and Aydin (1987) documented downward fracture propagation in lava flows due to cooling at the surface, with decreasing fracture intensities with increasing depth into flow interiors. Similarly, Pollard and Aydin (1988) provided an example of downward propagation of joints in a shale siltstone sequence, with many fractures terminating so that spacing increased down-section (Fig. 13 *in* Pollard and Aydin, 1988). However, in both cases, the resulting finite geometries did not display merging of fractures from upper zones into a single fracture down-section; instead, these downward-propagating fractures terminate without direct interaction with other fractures. Finally, to our

knowledge, there are no experimental studies that have documented fracture complex geometries like those presented here using the equivalent of a downward propagating system, with multiple fractures merging into a single fracture.

5.4 The role of branching in fracture network evolution and fluid flow pathways

Although fracture intensity increases up-section due to both the increase in the number of isolated fractures and the multiple fractures that branch upward (or splay) from single, planar fractures, we suggest that the latter mechanism best explains: 1) the exponential up-section increase in fracture intensity; 2) the higher C_v values at higher stratigraphic levels (Table 1; Fig. 9); and 3) the correlation of zones of higher intensity across stratigraphic levels (Fig. 9). Because the increase in F.I. is relatively linear within the lower, oxidized section (Scanlines 1-4), we also posit that, at least in part, branching in the bleached section explains the deviation from a linear F.I. increase within the bleached upper section. For instance, if we used the best-fit linear function based on F.I. data from Scanlines 1 through 4 (Fig. 9), we would predict a fracture intensity of 0.382 m^{-1} at 90 m above the base, instead of the 0.700 m^{-1} value documented for Scanline 8 (Table 1; Figs. 9 and 10).

Although not as vertically continuous as the fracture corridors described by Rogers et al. (2004) in nearby Zion National Park, the zones of elevated F.I. present at each stratigraphic level represent the localization of strain along tabular zones parallel to the joint set that are consistent with the elevated fracture intensities predicted by the modeling of Olson (2004). In a subsurface system with open fractures, these zones would permit enhanced fluid flow (e.g., Quistiaux et al., 2010). We can identify zones of elevated fracture intensity at all stratigraphic levels, where fluid flow might be localized, with a general increase in fracture corridors up section. However, at the highest stratigraphic levels (Scanlines 7 and 8), fracture intensities are

high enough that flow would likely become less focused and more diffuse but remain at high flow rates.

6. Implications

We suggest that upward fracture branching may be an under-appreciated mechanism that strongly influences network geometries and resulting permeability in massive subsurface sandstone reservoirs. At fracture propagation velocities above some critical value (e.g., $v_{cr} \geq$ ~0.4 Ralyleigh wave velocity), perhaps, but not necessarily associated with the dissipation of energy within the damage zone of an earthquake event, even small variations in mechanical behavior may provide the propagation instabilities necessary to initiate fracture branching. Because fracture branching results in an up-section exponential increase in fracture intensity as well as zones of spatially-elevated fracture intensities, subsurface reservoirs may display similar vertical changes in permeability and flow localization where total strain accommodation may not vary within the stratigraphic section.

ACKNOWLEDGEMENTS

Special thanks to Ashley Griffith, John Hooker, and an anonymous reviewer who all provided insightful and constructive feedback that greatly improved this publication. Funding was provided by a 2018-2019 Keck Geology Consortium Advanced Research Project Grant as part of an NSF-REU Award to the Keck Geology Consortium (EAR 1659322; PIs Wirth, K., and Davidson, C.). Funding was also provided by NSF Award 2042114 to PI Surpless. Finally, funding was provided by the Geosciences Department at Trinity University, including funding from the Roy and Tinker Funds to support undergraduate student research. We thank former undergraduate students Elizabeth Hartson, Hannah Mathy, Samuel Simoneau, Charlie Hankla, Madison Woodley, and Curtis Segarra, who provided excellent field and laboratory support early in this

project, and we thank Richard Silver, Trinity University Geosciences Technician, who provided technical support throughout this project.

References

Abraham, F.F., Brodbeck, D., Rafey, R., and Rudge, W., 1994, Instability dynamics of fracture: a computer simulation investigation: Physical Review Letters, v. 73, p. 272.

Agisoft Metashape, 2020, Agisoft Metashape User Manual, version 1.6 (pdf): accessed June, 2020, https://www.agisoft.com/pdf/metashape-pro_1_6_en.pdf.

Al-Masrahy, M. A., Melvin, J., Abdulatif, O., and Makkawi, M., 2012, Core and image log analysis of paleowind directions in the lower Permian Unayzah reservoir, subsurface central and eastern Saudi Arabia: American Association of Petroleum Geologists, Search and Discovery, Article 50734, pp. 1-4.

Al-Tahini, A.M., Sondergeld, C., and Rai, C.S., 2006, The effect of cementation on the mechanical properties of sandstones: SPE Reservoir Evaluation and Engineering, v. 9, p. 308-316.

Anderson, R.E., and Christenson, G.E., 1989, Quaternary faults, folds, and selected volcanic features in the Cedar City 1°x2° quadrangle, Utah: Utah Geological and Mineral Survey Miscellaneous Publication 89-6, 29 p.

Anderson, J.J., and Rowley, P.D., 1987, Geologic map of the Panguitch NW quadrangle, Iron and Garfield Counties, Utah: Utah Geological and Mineral Survey Map 103, 8 p. pamphlet, scale 1:24,000.

Aydin, A., 2000, Fractures, faults, and hydrocarbon entrapment, migration, and flow: Marine and Petroleum Geology, v. 17, p. 797–814.

Bai, T., and Pollard, D.D., 2000, Fracture spacing in layered rocks: a new explanation based on the stress transition: Journal of Structural Geology, v. 22, p. 43-57.

Barbier, M., Lepr^etre, R., Callot, J.-P., Gasparrini, M., Daniel, J.-M., Hamon, Y., Lacombe, O., and Floquet, M., 2012, Impact of fracture stratigraphy on the paleohydrogeology of the Madison Limestone in two basement-involved folds in the Bighorn basin, (Wyoming, USA): Tectonophysics, v. 576-577, p. 116-132.

Becker, A., and Gross, M., 1996, Mechanisms for joint saturation in mechanically layered rocks: an example from southern Israel: Tectonophysics, v. 257, p. 223 – 237.

Beitler, B., Parry, W.T., and Chan, M.A., 2005, Fingerprints of fluid flow - chemical diagenetic history of the Jurassic Navajo Sandstone, Southern Utah, U.S.A.: Journal of Sedimentary Research, v. 75, p. 547-561.

Ben-Zion, Y., 2001, Dynamic ruptures in recent models of earthquake faults: Journal of the Mechanics and Physics of Solids v. 49, p. 2209-2244.

Ben-Zion, Y., 2008, Collective behavior of earthquakes and faults: Continuum-discrete transitions, progressive evolutionary changes, and different dynamic regimes: Reviews of Geophysics, v. 46, doi: 10.1029/2008RG000260.

Bergbauer, S., and Pollard, D., 2004, A new conceptual fold-fracture model including prefolding joints, based on field data from the Emigrant Gap anticline, Wyoming: Geological Society of America Bulletin, v.116, p. 294 – 307.

Beroza, G., and Ide, S., 2011, Slow Earthquakes and Nonvolcanic Tremor: Annual Review of Earth and Planetary Sciences, v. 39, p. 271-296.

Bhat, H., Dmowska, R., King, G., Klinger, Y., and Rice, J., 2007, Off-fault damage patterns due to supershear ruptures with application to the 2001 Mw 8.1 Kokoxili (Kunlun) Tibet earthquake: Journal of Geophysical Research-Solid Earth, v. 112, B06301, 19 p.

Bhat, H. S., Rosakis, A. J., and Sammis, C. G., 2012, A micromechanics based constitutive model for brittle failure at high strain rates: Journal of Applied Mechanics, v. 79.

Bisdom, K., Bertotti, G., and Nick, H., 2016, The impact of different aperture distribution models and critical stress criteria on equivalent permeability in fractured rocks: Journal of Geophysical Research Solid Earth, v. 121, p. 4045-4063.

Bonnet, E., Bour, O., Odling, N.E., Davy, P., Main, I., Cowie, P.A., and Berkowitz, B., 2001, Scaling of fracture systems in geological media: Reviews in Geophysics, v. 39, p. 347-383.

Braunagel, M. J., & Griffith, W. A., 2022, Microstructural Controls on Mixed Mode Dynamic Fracture Propagation in Crystalline and Porous Granular Rocks: Journal of Geophysical Research, Solid Earth, v. 127, e2021JB022528.

Chalivendra, V.B., and Rosakis, A.J., 2008, Interaction of dynamic mode-I crack with inclined interfaces: Engineering Fracture Mechanics, v. 75, p. 2385–2397.

Chan, M. A., Parry, W.T., and Bowman, J.R., 2000, Diagenetic hematite and manganese oxides and fault-related fluid flow in Jurassic sandstones, southeastern Utah: AAPG Bulletin, v. 84, p. 1281– 1310.

Chau V.T., Bažant, Z.P., and Su, Y., 2016, Growth model for large branched three-dimensional hydraulic crack system in gas or oil shale: Philosophical Transactions of the Royal Society A, v. 374: 20150418.

Choi, J.-H., Edwards, P., Ko, K., Kim, Y.-S., 2016, Definition and classification of fault damage zones: a review and a new methodological approach: Earth Science Reviews, v. 152, p. 70–87.

Cooke, M., 1997, Predicting fracture localization in folded strata from mechanical stratigraphy and fold shape: a case study of East Kaibab monocline, Utah: International Journal of Rock Mechanics, v. 34, Paper 056.

Cooke, M. L., and Pollard, D. D., 1996, Fracture propagation paths under mixed mode loading within rectangular blocks of polymethyl methacrylate: Journal of Geophysical Research, Solid Earth, v. 101, p. 3387-3400.

Cooke, M., and Pollard, D., 1997, Bedding-plane slip in initial stages of fault-related folding: Journal of Structural Geology, v. 19, p. 567-581.

Cooke, M., Mollema, P., Pollard, D., and Aydin, A., 2000, Interlayer slip and joint localization in the East Kaibab Monocline, Utah: field evidence and results from numerical modeling, *In*: Cosgrove, J., and Ameen, M., Eds., Forced folds and fractures: Geological Society, London, Special Publications, v. 169, p. 23-49.

Cooke, M. L., and Underwood, C. A., 2001, Fracture termination and step-over at bedding interfaces due to frictional slip and interface opening: Journal of Structural Geology, v. 23, p. 223-238.

Couples, G., Lewis, H., 1998, Lateral variations in strain in experimental forced folds: Tectonophysics, v. 295, p. 79 – 91.

Cowie, P.A., and Scholz, C.H., 1992, Displacement-length scaling relationship for faults: Data synthesis and discussion: Journal of Structural Geology: v. 14, p. 1149–1156, doi:10.1016/0191-8141 (92)90066-6.

Corradetti, A., Tavani, S., Parente, M., Iannace, A., Vinci, F., Pirmez, C., Torrieri, S., Giorgioni, M., Pignalosa, A., and Mazzoli, S., 2018, Distribu Distribution and arrest of vertical through-going joints in a seismic-scale carbonate platform exposure (Sorrento peninsula, Italy):

insights from integrating field survey and digital outcrop model: Journal of Structural Geology, v. 108, p. 121-136.

Davis, G., 1999, Structural geology of the Colorado Plateau region of southern Utah, with special emphasis on deformation bands: Geological Society of America Special Paper 342, 157 p.

DeGraaff, J., and Aydin, A., 1987, Surface morphology of columnar joints and its significance to mechanics and direction of joint growth: Geological Society of America Bulletin, v. 99, p. 605-617.

DeWitt, E., Thompson, J., and Smith, R., 1986, Geology and gold deposits of the Oatman district, northwestern Arizona: U.S. Geologic Survey Open-File Report 86-0638, 34 p.

Dixon, S. A., Summers, D.M., and Surdam, R.C., 1989, Diagenesis and preservation of porosity in Norphlet Formation (Upper Jurassic), southern Alabama: AAPG Bulletin, v. 73, p. 707–728.

Dobereiner, L., 1984, Engineering Geology of Weak Sandstones: unpublished Ph.D. Thesis, Imperial College, London.

Doelling, H., 2008, Geologic Map of the Kanab 30' x 60' Quadrangle; Kane and Washington Counties, Utah, and Coconino and Mohave Counties, Arizona: Utah Geological Survey Miscellaneous Publication 08-2DM.

Doelling, H.H., and Davis, F.D., 1989, The geology of Kane County, Utah, with sections on petroleum and carbon diox-ide by Cynthia J. Brandt: Utah Geological and Mineral Sur-vey Bulletin 124, 192 p., scale 1:100,000, 10 plates.

Dyke, C.G., and Dobereiner, L., 1991, Evaluating the strength and deformability of sandstones: Quarterly Journal of Engineering Geology, v. 24, p. 123-134.

Engelder, T., and Fischer, M., 1996, Loading configurations and driving mechanisms for joints based on the Griffith energy-balance concept: Tectonophysics, v. 256, p. 253-277.

Engelder, T., 2007, Propagation velocity of joints: a debate over stable vs. unstable growth of cracks in the earth, *In* 5th Conference on the Fractography of Glasses and Ceramics, p. 457-482.

Evans, M.A., and Dunne, W.M., 1991, Strain factorization and partitioning in the North Mountain thrust sheet, central Appalachians, U.S.A.: Journal of Structural Geology, v. 13, p.21–35.

Ferrill, D.A., and Dunne, W.M., 1989, Cover deformation above a blind duplex: an example from West Virginia, U.S.A.: Journal of Structural Geology, v. 11, p. 421–431.

Field, J.E., 1971, Brittle fracture: its study and application: Contemporary Physics, v. 12, p. 1-31.

Fineberg, J., and Bouchbinder, E., 2015, Recent developments in dynamic fracture: some perspectives: International Journal of Fracture, v. 196, p. 33-57.

Flodin, E., and Aydin, A., 2004a, Faults with asymmetric damage zones in sandstone, Valley of Fire State Park, southern Nevada: Journal of Structural Geology, v. 26, p. 983-988.

Flodin, E., and Aydin, A., 2004b, Evolution of a strike-slip fault network, Valley of Fire State Park, southern Nevada: Geological Society Of America Bulletin, v. 116, p. 42-59.

Fonstad, M., Dietrich, J., Courville, B., Jensen, J., and Carbonneau, P., 2013, Topographic structure from motion: a new development in photogrammetric measurement: Earth Surface Processes and Landforms, v. 38, p. 421 – 430.

Fossen, H., Schultz, R., and Torabi, A., 2011, Conditions and implications for compaction band formation in the Navajo sandstone, Utah: Journal of Structural Geology, v. 33, p. 1477-1490.

Freund, L., 1990, Dynamic fracture mechanics: Cambridge, England, Cambridge University Press, 563 p.

Gillespie, P.A., Johnston, J.D., Loriga, M.A., McCaffrey, K.J.W., Walsh, J.J., and Watterson, J., 1999, Influence of layering on vein systematics in line samples, In: McCaffrey, K.J.W., Lonergan, L., Wilkinson, J.J. (Eds.), Fractures, Fluid Flow and Mineralization: Geological Society, London, Special Publications 155, p. 35-56.

Griffith, W.A., Rosakis, A., Pollard, D.D., and Ko, C.W., 2009, Dynamic rupture experiments elucidate tensile crack development during propagating earthquake ruptures: Geology v. 37, p. 795–798.

Gross, M.R., 1993, The origin and spacing of cross joints: examples from the Monterey Formation, Santa Barbara Coastline, California: Journal of Structural Geology, v. 15, p. 737-751.

Gross, M., Fischer, M., Engelder, T., and Greenfield, R., 1995, Factors controlling joint spacing in interbedded sedimentary rocks: Integrating numerical models with field observations from the Monterey Formation, U.S.A., In Ameen, M., Ed., Fractography: Fracture topography as a tool in fracture mechanics and stress analysis: Geological Society Special Publication, v. 92, p. 215 – 233.

Hankla, C., and Judge, S.., 2019, An analysis of fractures around the Sevier fault zone in Red Hollow Canyon near Orderville, Utah: Keck Geology Consortium, Volume of Short Contributions, v. 32, 7 p.

Harrington, S., Teitelman, J., Rummel, E., Morse, B., Chen, P., Eisentraut, D., and McDonough, D., 2017, Validating Google Earth Pro as a Scientific Utility for Use in Accident Reconstruction: International Journal of Transportation Safety, v. 5, doi:10.4271/2017-01-9750.

Hickman, R.G., Varga, R.J., and Altany, R.M., 2009. Structural style of the marathon thrust belt, West Texas: Journal of Structural Geology, v. 31, p. 900–909.

Hooker, J.N., Laubach, S.E., and Marrett, R., 2013, Fracture-aperture sized frequency, spatial distribution, and growth processes in strata-bounded and non-strata- bounded fractures, Cambrian Meson Group, NW Argentina: Journal of Structural Geology, v.54, p.54-71.

Hooker, J., Laubach, S., and Marrett, R., 2018, Microfracture spacing distributions and the evolution of fracture patterns in sandstones: Journal of Structural Geology, v. 108, p. 66-79.

Isida, M., and Noguchi, H., 1992, Stress intensity factors at tips of branched cracks under various loadings: International Journal of Fracture, v. 54, p. 293–316.

Johnson, K., Nissen, E., Saripalli, S., Arrowsmith, R., McGarey, P., Scharer, K., Williams, P., and Blisnuik, K., 2014, Rapid mapping of ultrafine fault zone topography with structure from motion: Geosphere, v. 10, p. 969 – 986.

Kattenhorn, S. A., Aydin, A., and Pollard, D. D., 2000, Joints at high angles to normal fault strike: an explanation using 3-D numerical models of fault-perturbed stress fields: Journal of Structural Geology, v. 22, p. 1-23.

Kim, Y.-S., Peacock, D.C.P., Sanderson, D.J., 2003. Strike-slip faults and damage zones at Marsalforn, Gozo Island, Malta: Journal of Structural Geology, v. 25, p. 793–812.

Kim, Y.-S., Peacock, D.C.P. and Sanderson, D.J., 2004, Fault damage zones: Journal of Structural Geology, v. 26, p. 503–517.

Kim, Y., and Sanderson, D., 2006, Structural similarity and variety at the tips in a wide range of strike–slip faults: a review: Terra Nova, v. 18, p. 330-344.

Knipe, R.J., Jones, G., and Fisher, Q.J., 1998, Faulting, fault sealing and fluid flow in hydrocarbon reservoirs: an introduction. In: Jones, G., Fisher, Q.J., Knipe, R.J. (Eds.), Faulting, Fault Sealing and Fluid Flow in Hydrocarbon Reservoirs: Geological Society of London Special Publication, 147, pp. vii–xxi.

Kulander, B.R., and Dean, S.L., 1995, Observations on fractography with laboratory experiments for geologists, In M.S. Ameen, Ed., Fractography: Fracture Topography as a Tool in Fracture Mechanics and Stress Analysis, Geological Society Special Paper 92, p. 97-147

Ladeira, F.L., and Price, N.J., 1981, Relationship between fracture spacing and bed thickness: Journal of Structural Geology, v. 3, p. 179-183.

Laubach, S., Olson, J., and Gross, M., 2009, Mechanical and Fracture Stratigraphy: AAPG Bulletin, v. 93, p. 1413-1426.

Laubach, S., Lander, R., Criscenti, L., Anovitz L., Urai, J., Pollyea R., Hooker, J., Narr, W., Evans, M., Kerisit, S., Olson, J., Dewers, T., Fisher, D., Bodnar, R., Evans, B., Dove, P., Bonnell, L., Marder, M., and Pyrak-Nolte, L., 2019, The Role of Chemistry in Fracture Pattern Development and Opportunities to Advance Interpretations of Geological Materials: Reviews of Geophysics, v. 57, p. 1065-1111.

Lowe, D., 2004, Distinctive image features from scale invariant keypoints: International Journal of Computer Vision, v. 60, p. 91–110, doi: 10 .1023 /B: VISI .0000029664 .99615.94.

Lund, W.R., Knudsen, T.R., and Vice, G.S., 2008, Paleoseismic reconnaissance of the Sevier fault, Kane and Garfield Counties, Utah: Utah Geologic Survey Special Study 122, Paleoseismology of Utah, v. 16, 31 p.

Maniatis, G., and Hampel, A., 2008, Along-strike variations of the slip direction on normal faults: Insights from three-dimensional finite-element models: Journal of Structural Geology, v. 30, p. 21-28.

Marder, M., and Fineberg, J., 1996, How things break: Physics Today, v. 49, p. 24-29.McGinnis, R.N., Ferrill, D.A., Smart, K.J., Morris, A.P., Higuera-Diaz, C., and Prawica, D., 2015, Pitfalls of using entrenched fracture relationships. Fractures in bedded carbonates of the Hidden Valley fault zone, Canyon Lake Gorge, Comal County, Texas: American Association of Petroleum Geologists Bulletin, v. 99, p. 2221-2245.

McGrath, A.G., and Davison, I., 1995, Damage zone geometry around fault tips: Journal of Structural Geology, v. 17, p. 1011–1024.

McKie, T., Jolley,S.J., and Kristensen, M.B., 2010, Stratigraphic and structural compartmentalization of dryland fluvial reservoirs: Triassic Heron Cluster, central North Sea: Geological Society of London, Special Publication, v. 347, pp. 165-198

Melosh, B., Rowe, C., Smit, L., Groenewald, C., Lambert, C., and Macey, P., 2014, Snap, Crackle, Pop: Dilational fault breccias record seismic slip below the brittle–plastic transition: Earth and Planetary Science Letters, v. 403, p. 432-445.

Mitchell, T. M., and Faulkner, D. R., 2009, The nature and origin of off-fault damage surrounding strike-slip fault zones with a wide range of displacements: A field study from the Atacama fault system, northern Chile: Journal of Structural Geology, v 31, p. 802-816.

Morse, D., 1994, Silicilastic Reservoir rocks, In: Magoon, L., and Dow, W. (Eds.), The petroleum system; from source to trap: American Association of Petroleum Geologists, v. 60, p. 121-139.

Muller, O. H., and Pollard, D. D., 1977, The stress state near Spanish Peaks, Colorado, determined from a dike pattern: Pure and Applied Geophysics, v. 115, p. 69–86.

Narr, W., Schechter, D.W., Thompson, L.B., 2006, Naturally Fractured Reservoir characterization: Society of Petroleum Engineers, Richardson, Texas, 115 p.

Narr, W., and Suppe, J., 1991, Joint spacing in sedimentary rocks: Journal of Structural Geolology, v. 13, p. 1037-1048.

Nickling, W.G., Neuman, C.M., and Lancaster, N., 2002, Grainfall processes in the lee of transverse dunes, Silver Peak, Nevada: Sedimentology, v. 49, p. 191–209, doi:10.1046/j.1365-3091.2002.00443.x.

Nielsen, G.B., Chan, M.A., and Petersen, E.U., 2009, Diagenetic Coloration Facies and Alteration History of the Jurassic Navajo Sandstone, Zion National Park and Vicinity, Southwestern Utah: *In* Geology and Geologic Resources and Issues of Western Utah, Utah Geological Association, No. 38, p. 67-96.

Nelson, R.A., 2001. Geologic Analysis of Naturally Fractured Reservoirs, 2nd edition. Gulf Professional Publishing, Boston.

Nunes, A.L., 1989, Um Estodo Sobre as Caracteristicas de Resistencia e Deformabilidade de Arenitos. Unpublished M.S. Thesis, Pontificia Universidade Catolica de Rio de Janeiro.

Odonne, F., Lezin, C., Massonnat, G., and Escadeillas, G., 2007, The relationship between joint aperture, spacing distribution, vertical dimension and carbonate stratification: an

example from the Kimmeridgian limestones of Pointe-du-Chay (France): Journal of Structural Geology, v. 29, p. 746-758.

Olson, J.E., 2003. Sublinear scaling of fracture aperture versus length: an exception or the rule?: Journal of Geophysical Research, v. 10. https://doi.org/10.1029/2001JB000419.

Olson, J., 2004, Predicting fracture swarms – the influence of subcritical crack growth and the crack-tip process zone on joint spacing in rock, In Cosgrove, J., and Engelder, T. (eds.), The intiation, Propagation, and Arrest of Joints and Other Fractures: Geological Society of London, Special Publication 231, p. 73-87.

Olson, J. E., and Pollard, D. D., 1989, Inferring paleostress from natural fracture patterns: A new method: Geology, v. 17, p. 345–348.

Olson, J., and Pollard, D., 1991, The initiation and growth of en echelon veins: Journal of Structural Geology, v. 13, p. 595 – 608.

Parry, W.T., Chan, M.A., and Beitler, B., 2004, Chemical bleaching indicates episodes of fluid flow in deformation bands in sandstone: American Association of Petroleum Geologists Bulletin, v. 88, p. 175-191.

Peacock, D.C.P., Dimmen, V., Rotevatn, A., and Sanderson, D.J., 2017, A broader classification of damage zones: Journal of Structural Geology, v. 102, p. 179–192.

Peterson, F., and Pipiringos, G., 1979, Stratigraphic relations of the Navajo Sandstone to Middle Jurassic formations, southern Utah and northern Arizona: Professional Paper, doi: 10.3133/pp1035b.

Petit JP., Auzias V., Rawnsley K., and Rives T., 2000, Development of joint sets in the vicinity of faults, *In* Lehner F.K., Urai J.L. (eds): Aspects of Tectonic Faulting, Springer, Berlin https://doi.org/10.1007/978-3-642-59617-9_9.

Petit, J.P., and Barquins, M., 1988, Can natural faults propagate under mode-II conditions?: Tectonics, v. 7, p. 1243–1256.

Pollard, D.D., and Aydin, A., 1988, Progress in understanding jointing over the past century: Geological Society pf America Bulletin, v. 100, p. 1181-1204.

Pollard, D., Segall, P., and Delaney, P., 1982, Formation and interpretation of dilatant echelon cracks: Geological Society of America Bulletin, v. 93, p. 1291-1303.

Pollard, D., and Segall, P., 1987, Theoretical displacements and stresses near fractures in rock: with applications to faults, joints, veins, dikes, and solution surfaces, *In* Atkinson, B. (ed.), Fracture Mechanics of Rock: Academic Press, London, p. 377-350.

Price, N., 1959, Mechanics of jointing in rocks: Geological Magazine, v. 96, p. 149 – 167.

Price, N., and Cosgrove, J., 1990, Analysis of Geological Structures: Cambridge University Press, Cambridge, 502 p.

Questiaux, J-M., Couples, G., and Ruby, N., 2010, Fractured reservoirs with fracture corridors: Geophysical Prospecting, v. 58, p. 279-295.

Rabimi-Aghdam, S., Chau, V-T, Lee, H., Nguyen, H., Li, W., Karra, S., Rougier, E., Viswanathan, H., Srinivasan, G., and Bazant, Z.P., 2019, Branching of hydraulic cracks enabling permeability of gas or oil shale with closed natural fractures: Proceedings of the National Academy of Sciences, v. 116, p. 1522-1537.

Ramulu, M., and Kobayashi, A.S., 1984, Criteria for Dynamic Crack Curving and Branching: Fracture, v. 84, p. 3099–3107, doi: 10.1016/b978-1-4832-8440-8.50330-6.Ravi-Chander and Knauss, 1984a; 1984b

Ramulu, M., and Kobayashi, 1985, Mechanics of crack curving and branching – a dynamic fracture analysis: International Journal of Fracture, v. 27, p. 187-201.

Ravi–Chandar, K., and Knauss, W., 1984a, An experimental investigation into dynamic fracture: II. Microstructural aspects: International Journal of Fracture, v. 26, p. 65-80.

Ravi–Chandar, K., and Knauss, W., 1984b, An experimental investigation into dynamic fracture: III. On steady-state crack propagation and crack branching: International Journal of Fracture, v. 26, p. 141–154.

Reber, S., Taylor, W., Stewart, M., and Schiefelbein, I., 2001, Linkage and Reactivation along the northern Hurricane and Sevier faults, southwestern Utah, In M.C. Erskine, J.E. Faulds, J.M. Bartley, and P.D. Rowley, Eds., The Geologic Transition, High Plateaus to Great Basin – A Symposium and Field Guide, The Mackin Volume: Utah Geological Association Publication 30, Pacific Section American Association of Petroleum Geologists Publication GB78, p. 379 – 400.

Reches, Z., and Lockner, D., 1994, Nucleation and growth of faults in brittle rocks: Journal of Geophysical Research – Solid Earth, v. 99, p. 18,159 - 18,173.

Rives, T., Razack, M., Petit, J., and Rawnsley, K., 1992, Joint spacing: analogue and numerical simulations: Journal of Structural Geology, v. 14, p. 925-937.

Robinson, D., Brough, C. and S. Das, S., 2006, The Mw 7.8, 2001 Kunlunshan earthquake: Extreme rupture speed variability and effect of fault geometry: Journal of Geophysical Research-Solid Earth v. 111, B08303, doi: 10.1029/2005JB004137.

Rogers, C., Myers, D., and Engelder, T., 2004, Kinematic implications of joint zones and isolated joints in the Navajo Sandstone at Zion National Park, Utah: Evidence for Cordilleran relaxation: Tectonics, v. 23, TC1007, doi:10.1029/2001TC001329.

Rosakis, A. J., and Ravichandran, G., 2000, Dynamic failure mechanics: International journal of solids and structures, v. 37, p. 331-348.

Rowley, P., 1998, Cenozoic transverse zones and igneous belts in the Great Basin, Western United States: Their tectonic and economic implications In Faulds, J.E., and Stewart, J.H., Eds., Accommodation zones and transfer zones: the regional segmentation of the Basin and Range province: Geological Society of America Special Paper No. 343, p. 195-228.

Sagy, A., Reches, Z., and Roman, I., 2001, Dynamic fracturing: field and experimental observations: Journal of Structural Geology, v. 23, p. 1223-1239.

Sargent, K.A. and Philpott, B.C., 1987, Geologic map of the Kanab quadrangle. Kane County, Utah, and Mohave and Coconino Counties, Arizona: U.S. Geological Survey Map GQ-1603.

Savalli, L., and Engelder, T., 2005, Mechanisms controlling rupture shape during subcritical growth of joints in layered rock: Geological Society of America Bulletin, v. 117, p. 436-449.

Schiefelbein, I.M., 2002, Fault segmentation, fault linkage, and hazards along the Sevier fault, southwestern Utah [M.S. thesis]: Las Vegas, University of Nevada at Las Vegas, 132 p.

Schulz, R.A., 2019, Geologic Fracture Mechanics: Cambridge University Press, Cambridge, U.K., 592 p.

Segall, P., and Pollard, D.D., 1983, Joint formation in granitic rock of the Sierra Nevada: Geological Society of America Bulletin, v. 94, p. 563-575.

Sharon, E. and Fineberg, E., 1996, Microbranching instability and the dynamic fracture of brittle materials: Physical Review B, v. 54, p. 7128-7139.

Shukla, A., Nigam, H., and Zervas, H., 1990, Effect of Stress Field Parameters on Dynamic Crack Branching: Engineering Fracture Mechanics, v. 36, p. 429–438, doi: 10.1016/0013-7944(90)90290-w.

Smart, K., Ferrill, D., and Morris, A., 2009, Impact of interlayer slip on fracture prediction from geomechanical models of fault-related folds: American Association of Petroleum Geologists Bulletin, v. 93, p. 1447 – 1458.

Smart, K., Ferrill, D., Morris, A., McGinnis, R., 2012, Geomechanical modeling of stress and strain evolution during contractional fault-related folding: Tectonophysics, v. 576-577, p. 171-196.'

Song, J-H., Wang, H., and Belytschko, T., 2008, A comparative study on finite element methods for dynamic fracture: Computational Mechanics, v. 42, p. 239-259.

Stewart, M., and Taylor, W., 1996, Structural analysis and fault segment boundary identification along the Hurricane fault in southwestern Utah: Journal of Structural Geology, v. 18, p. 1017 – 1029.

Sundaram, B., and Tippur, H., 2016, Dynamics of crack penetration vs. branching at a weak interface: an experimental study: Journal of the Mechanics and Physics of Solids, v. 96, p. 312-332.

Surdam, R. C., Jiao, Z. S., and MacGowan, D. B., 1993, Redox reactions involving hydrocarbons and mineral oxidants: A mechanism for significant porosity enhancement in sandstones: AAPG Bulletin, v. 77, p. 1509–1518.

Surpless, B., and Wigginton, 2020, The impact of inter-bed cohesion on fold-related fracture development, Stillwell anticline, west Texas (USA): Journal of Structural Geology, v. 134, doi: 10.1016/j.jsg.2019.103974.

Thelin, G.P., and Pike, R.J., 1991, Landforms of the Conterminous United States - A Digital Shaded-Relief Portrayal: U.S.G.S. Geologic Investigations Series I – 2720.

Turner, P., 1980, Continental red beds: New York, Elsevier, 562 p.

Underwood, C., Cooke, M., Simo, J., and Muldoon, M., 2003, Stratigraphic controls on vertical fracture patterns in Silurian dolomite, northeastern Wisconsin: AAPG Bulletin, v. 87, p. 121-142.

Vermilye, J.M., and Scholz, C.H., 1999, Fault propagation and segmentation: insight from the microstructural examination of a small fault: Journal of Structural Geology, v. 21, p. 1623–1636.

Walker, T. R., Waugh, B., and Crone, A.J., 1978, Diagenesis in first cycle desert alluvium of Cenozoic age, south-western United States and north-western Mexico: Geological Society of America Bulletin, v. 89, p. 19– 32.

Wallner, H., 1939, Linienstrukturen au Bruchflachen: Zietschrift fur Physik, v. 114, p. 368-378.

Wennberg, O.P., Azizzadeh, M., Aqrawi, M.M., Blanc, E., Brockbank, P., Lyslo, K.B., Pickard, N., Salem, L.D., and Svånå, T., 2007, The Khaviz Anticline: an outcrop analogue to giant fractured Asmari Formation reservoirs in SW Iran. In: Lonergan, L., Jolly, R.J.H., Rawnsley, K., Sanderson, D.J. (Eds.), Fractured Reservoirs. Geological Society of London Special Publications, v. 270, p. 23-42.

Westoby, M.J., Brasington, J., Glasser, N.F., Hambrey, M.J., Reynolds, J.M., 2012, Structure-from-Motion photogrammetry: a low-cost, effective tool for geoscience applications: Geomorphology, v. 179, p. 300-314. doi: 10.1016/j.geomorph.2012.08.021.

Xu, L.R., Hung, Y.Y., and Rosakis, A.J., 2003, Dynamic crack deflection and penetration at interface in homogeneous materials: experimental studies and model predictions: Journal of the Mechanics and Physics of Solids, v. 51, p. 461–486.

Younes, A., and Engelder, T., 1999, Fringe cracks: Key structures for the interpretation of the progressive Alleghanian deformation of the Appalachian plateau: Geological Society of America Bulletin, v. 111, p. 219-239.

Zhang, P., Slemmons, D.B., and Mao, F., 1991, Geometric pattern, rupture termination and fault segmentation of the Dixie Valley– Pleasant Valley active normal fault system, Nevada, U.S.A.: Journal of Structural Geology, v. 13, p. 165–176.

Zhou, S., Zhuang, X., Zhu, H., and Rabczuk, T., 2018, Phase field modeling of crack propagation, branching and coalescence in rocks: Theoretical and Applied Fracture Mechanics, v. 96, p. 174-192.

FIGURE CAPTIONS:

Figure 1. Physiographic context for the Sevier fault zone study area within the Basin and Range-Colorado Plateau transition zone (see inset). In combination with the Grand Wash, Hurricane, and Paunaugunt faults, the Sevier-Toroweap fault accommodates extension across the transition zone. Ball is on the hanging wall of the west-dipping faults. Detailed structure of the study area (boxed) is displayed in Figure 2. Digital shaded relief modified from Thelin and Pike (1991). Figure significantly modified from Reber et al. (2001).

Figure 2. Structure map of the fault network within the Orderville geometric bend of the Sevier fault zone. Thick yellow lines are primary segments of the Sevier fault zone. Green shading indicates outcrop extent of the Jurassic Navajo Sandstone (Jn). Ball symbols on hanging wall of normal faults. Faults shown here are based primarily on mapping performed by Schiefelbein (2002) and our mapping, at 1:12,000 scale or larger. We developed a virtual outcrop model (VOM) based on image data from the area outlined in white (VOM area). We indicate the dominant fracture direction in the VOM area and the area to the northwest with black joint symbols.

Figure 3. Outcrop characteristics of the Jurassic Navajo Sandstone. **A.** View of contact between two thick (>10 m) crossbed sets present in outcrop. White dashed lines represent interdune depositional contact, with finer grained material than crossbeds above and below. South-dipping crossbeds are tabular and 5-15 cm thick. People for scale. **B.** Variation in crossbedding thicknesses are common near the contact between crossbed sets. Dashed line is an unusually sharp contact between crossbed sets, with beds in the upper set that appear to truncate those in the lower set, suggesting an erosional surface. Lens cap (8 cm diameter) for scale.

Figure 4. Examples of fracture geometries in field area. **A.** Three planar WNW-dipping normal faults subparallel to the Spencer Bench segment. The strike of these faults is similar to fractures that do not display observable shear displacement. **B.** Ground-based, oblique view of the vertical fracture network. Note the increase in fracture intensity from ground level to the top of the ridgeline. The scale bar shown in the image is accurate only in the foreground. **C.** Smaller-scale view of the image displayed in B. Note the localized zones of intense fracturing indicated by black arrows. **D.** Stacked series of crossbed sets (I-VI, divided by black dotted lines) in the footwall of the Spencer Bench fault segment (see Fig. 2 for location). Fracture network characteristics vary within sets, across set contacts, and even across individual crossbed contacts within a given set. Scale is approximate**.**

Figure 5. Fracture branching in outcrop. **A.** Uninterpreted fracture network on the cm- to dm-scale. **B.** Same fracture network displayed in A, with solid lines that indicate well-exposed fractures and dashed lines representing inferred fracture locations. Note that splays stem from a single, relatively planar, throughgoing fracture. **C.** Still image captured from UAV-based video of the same outcrop used to build the VOM model displayed in Figs. 6 and 7. White circles indicate loci of fracture branching, and fracture complexes 3 and 4 are displayed in Figures 7 and 8. Fracture complexes indicated by 5* are subsidiary fracture branches in the upper portion of fracture complex 5 (Fig. 8B). Black, dashed lines indicate prominent cross-bed set boundaries.

Figure 6. Plan view of the virtual outcrop model (VOM), with fracture traces on the continuous northeast cliff exposure shown in yellow and the Spencer Bench fault segment displayed with a red, dashed line. White dashed line marks break in slope, from steep, well-exposed outcrop to a shallow, poorly-exposed topographic bench (see text for discussion). We collected ground-

based data at the canyon floor from accessible fractures along the path displayed with the white dotted line. Equal-area stereonet displays fracture orientations from approximately 150 m of ground-based scanline data. The orthomosaic of the northeast canyon wall, displayed in Figure 7, represents VOM data projected onto a vertical plane oriented parallel to the VOM scanline orientation shown above, at N30°W.

Figure 7. Orthomosaic image of VOM, displaying locations of each scanline and model-mapped fractures (blue lines). Image (from VOM) projected onto vertical plane oriented N30°W (see Fig. 6). VOM-based scanlines are spaced at 10-m intervals, with Line 1 at approximately 20 m elevation above the ground-based field scanline. All scanlines are 260 m in length. White dots indicate prominent fracture branching initiation points, and yellow dots indicate branching geometries documented in Fig. 8. Histogram (right) displays vertical distribution of branching initiation points. White box outlines area displayed in Figure 5C. Image altered to brighten the central region, which was in shadow at the time of UAV image capture.

Figure 8. Representative "tree-like" fracture branching geometries along steeply dipping fractures (location of each branching geometry indicated on Fig. 7). Beside each geometry, we include the number of branch junctions (n) as well as the average and standard deviation for all branch angles. A. displays four examples of branching geometries traced from photos or VOM. In these diagrams, the initial primary fracture is bold and the bold gray line in 4 represents is a fracture against which two fractures terminate. The upward extents of most fractures in 1 - 3 cannot be traced higher due to poor exposure near the top of the study outcrop. B. dipslays branching geometry that extends from near the base of the outcrop to the top of the exposure (~80 meters vertical exposure). C. displays representative tree-like branching geometry of Sagy et al. (2001) (modified from Fig. 4a in Sagy et al., 2001).

Figure 9. Scanline data from 9 stratigraphic levels, measured relative to the approximate base of the VOM in Red Hollow Canyon. Field-based coloration of the Jurassic Navajo sandstone is displayed on the left. Graphical fracture distributions are displayed at the bottom of each scanline box, and normalized fracture intensities are shown above each fracture distribution. Values were smoothed across 5-fracture populations then normalized relative to that scanline's average fracture intensity. A value of 1 on each graph represents the average fracture intensity value shown to the right. Fracture data are summarized in Table 1. Data from ground-based observations are displayed at the bottom, with VOM-derived scanlines 1-8 shown with increasing elevation.

Figure 10. Changes in fracture intensity with stratigraphic position. Scanlines 1-3 are from the red, oxidized zone, scanlines 4 and 5 are from the transitional zone, and scanlines 6-8 are from the bleached zone of the Navajo Sandstone (Fig. 7). All VOM-based scanline data suggest a strong exponential relationship between stratigraphic position and fracture intensity (R^2=0.967).

Figure 11. Proposed model for natural fracture branching in the Jurassic Navajo Sandstone. **A.** Generalized diagram of gradual twist-hackle formation during upward propagation of the parent fracture in a mixed-mode I-III loading configuration (see Mode III loading arrows). Front face of block diagram represents the parent fracture plane. Although parent fracture tipline instability leads to twist hackle initiation, we suggest that the parent fracture continued to propagate upward in concert with upward and lateral hackle propagation and the intitaion of new twist hackle at higher stratigraphic levels. Figure significantly modified from Younes and Engelder (1999) and Pollard et al. (1982). **B.** Diagram of branched fracture complex "3" on Fig.

8A, which represents the finite geometry of the system. The bold line represents the parent fracture. We suggest the non-terminating upward parent fracture propagation prohibits any significant lateral hackle propagation across the parent fracture plane.

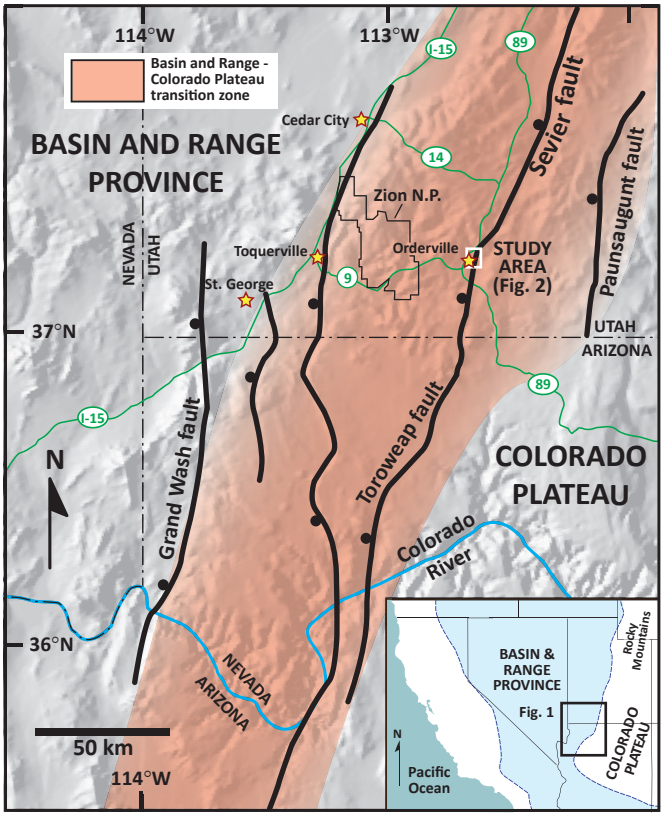

Figure 1. Physiographic context for the Sevier fault zone study area within the Basin and Range-Colorado Plateau transition zone (see inset). In combination with the Grand Wash, Hurricane, and Paunaugunt faults, the Sevier-Toroweap fault helps accommodate extension across the transition zone. Ball is on the hanging wall of the west-dipping faults. Detailed structure of the study area (boxed) is displayed in Figure 2. Digital shaded relief modified from Thelin and Pike (1991). Figure significantly modified from Reber et al. (2001).

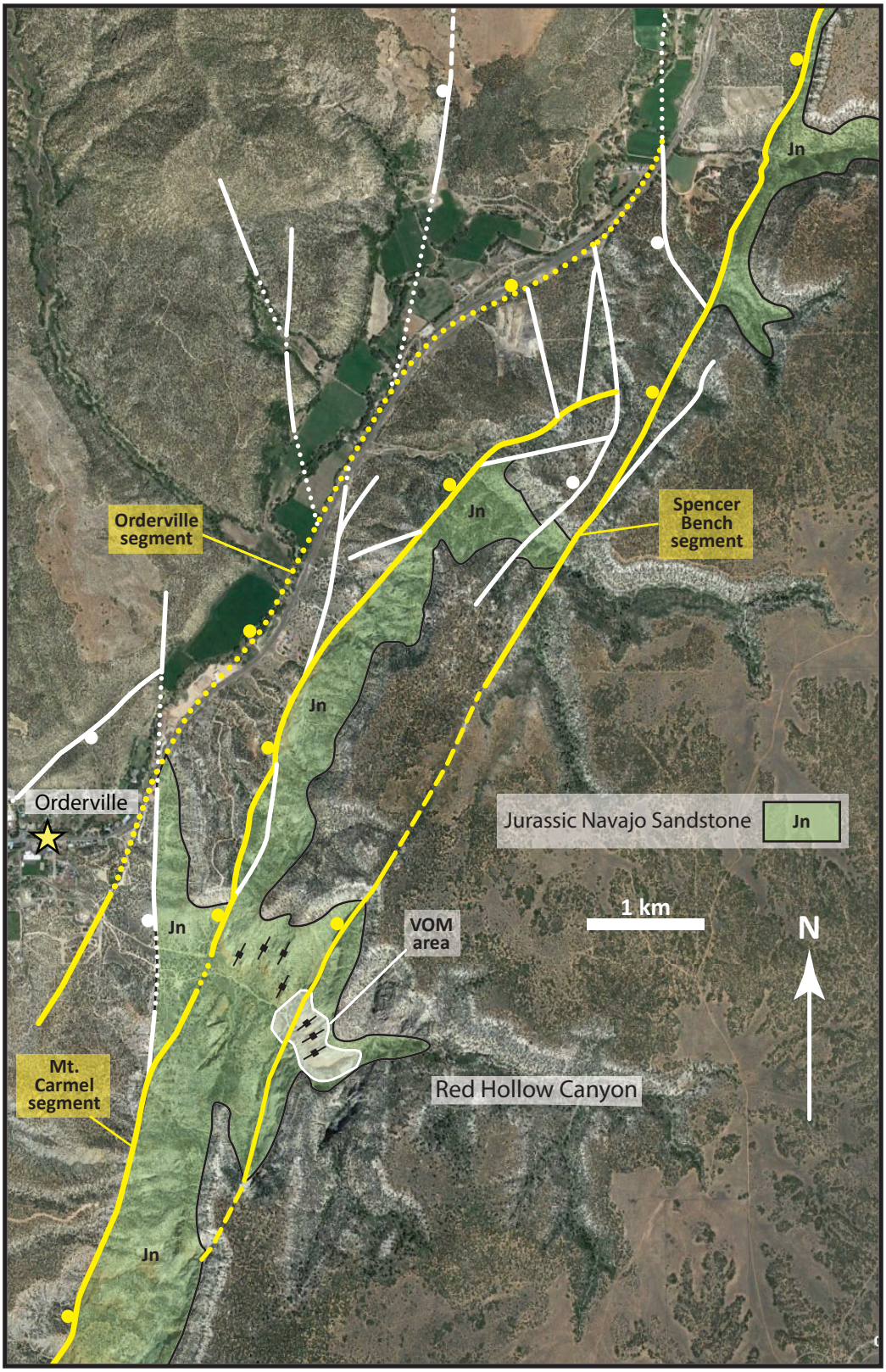

Figure 2. Structure map of the fault network within the Orderville geometric bend of the Sevier fault zone. Thick yellow lines are primary segments of the Sevier fault zone. Green shading indicates outcrop extent of the Jurassic Navajo Sandstone (Jn). Ball symbols on hanging wall of normal faults. Faults shown here are based primarily on mapping performed by Schiefelbein (2002) and our mapping, at 1:12,000 scale or larger. We developed a virtual outcrop model (VOM) based on image data from the area outlined in white (VOM area). We indicate the dominant fracture direction in the VOM area and the area to the northwest with black joint symbols.

Figure 3. Outcrop characteristics of the Jurassic Navajo Sandstone. A. View of contact between two thick (>10 m) crossbed sets present in outcrop. White dashed lines represent interdune depositional contact, with finer grained material than in crossbeds above and below. South-dipping crossbeds are tabular and 5-15 cm thick. People for scale. **B.** Variation in crossbedding thicknesses are common near the contact between crossbed sets. Dashed line is an unusually sharp contact between these crossbed sets, with beds in the upper set that appear to truncate those in the lower set, suggesting an erosional surface. Lens cap (8 cm diameter) for scale.

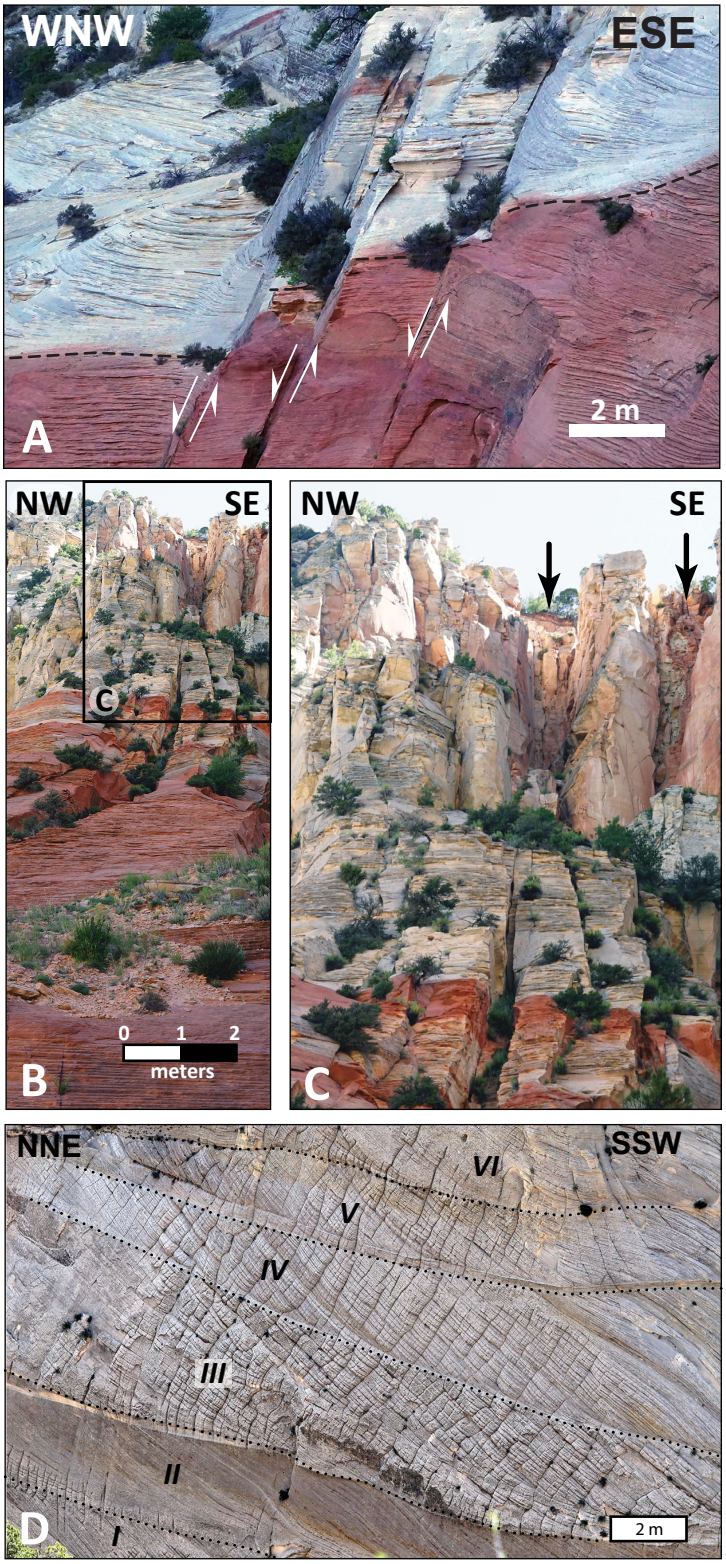

Figure 4. Examples of fault and fracture observations in the field area. **A.** Three planar, WNW-dipping normal faults subparallel to the Spencer Bench segment. The strike of these faults is similar to fractures that do not display observable shear displacement. **B.** Ground-based, oblique view of the vertical fracture network. Note the increase in fracture intensity from ground level to the top of the ridgeline. The scale bar shown in the image is accurate only in the foreground. **C.** Smaller-scale view of the image displayed in **B**. Note the localized zones of intense fracturing indicated by black arrows. **D.** Stacked series of crossbed sets (I-VI, divided by black dotted lines) in the footwall of the Spencer Bench fault segment (see Fig. 2 for location). Fracture network characteristics vary within sets, across set contacts, and even across individual crossbed contacts within a given set. Scale is approximate.

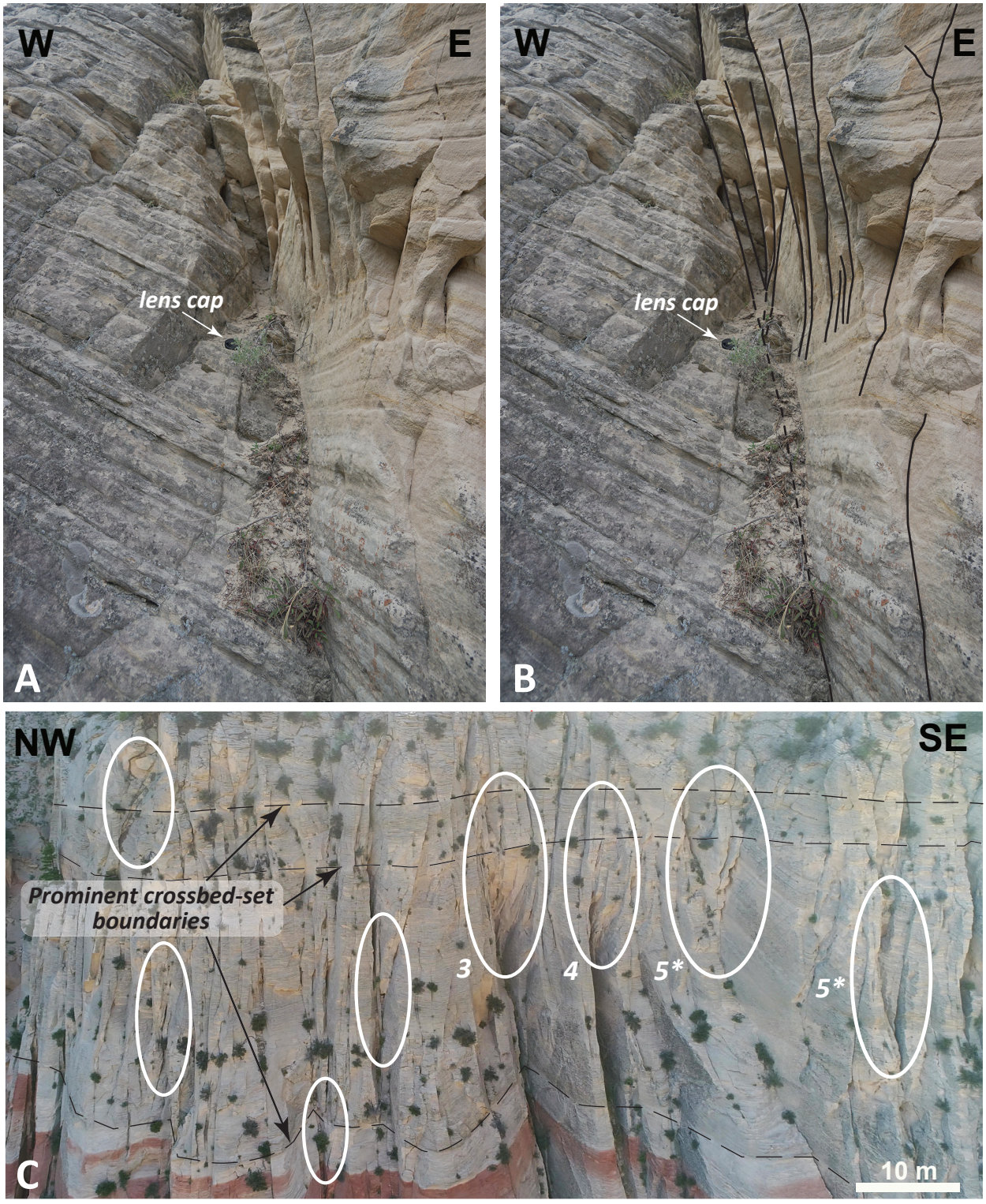

Figure 5. Fracture branching in outcrop. A. Uninterpreted fracture network in tabular crossbeds on the cm- to dm-scale. Lens cap (8 cm diameter) for scale. **B.** Same fracture network displayed in A, with solid lines that indicate well-exposed fractures and dashed lines representing inferred fracture locations. **C.** Still image captured from UAV-based video of the same outcrop used to build the VOM model displayed in Figures 6 and 7. White circles indicate loci of fracture branching, and fracture complexes 3 and 4 are displayed in Figures 7 and 8. Fracture complexes indicated by 5* are subsidiary fracture branches in the upper portion of fracture complex 5 (Fig. 8B). Black, dashed lines indicate prominent cross-bed set boundaries.

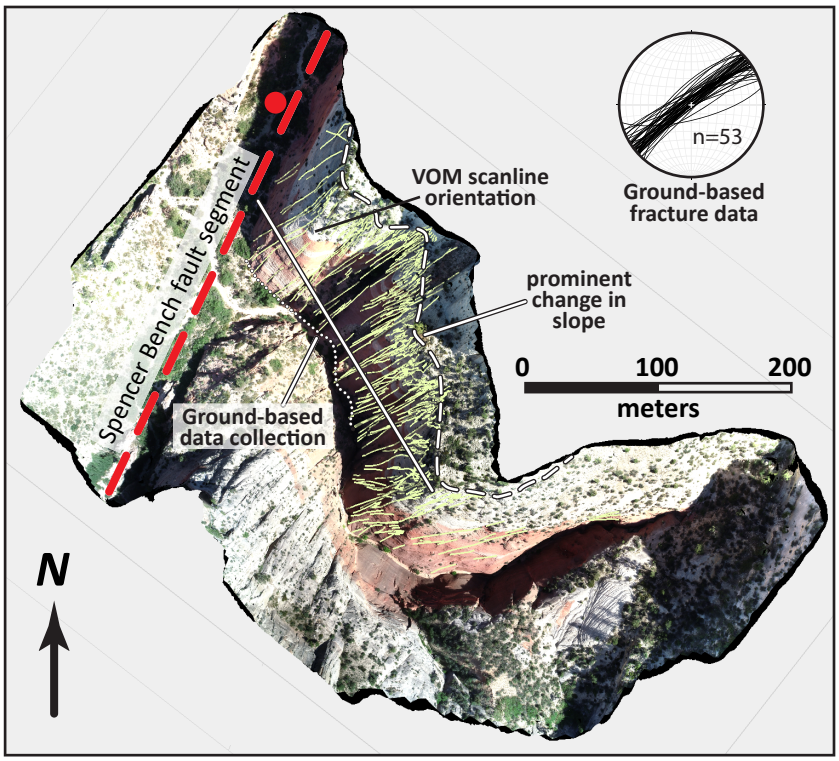

Figure 6. Plan view of the virtual outcrop model (VOM), with fracture traces on the continuous northeast cliff exposure shown in yellow and the Spencer Bench fault segment displayed with a red, dashed line. White dashed line marks break in slope, from steep, well-exposed outcrop to a shallow, poorly-exposed topographic bench (see text for discussion). We collected ground-based data at the canyon floor from accessible fractures along the path displayed with the white dotted line. Equal-area stereonet displays fracture orientations from approximately 150 m of ground-based scanline data. The orthomosaic of the northeast canyon wall, displayed in Figure 7, represents VOM data projected onto a vertical plane oriented parallel to the VOM scanline orientation shown above, at N30°W.

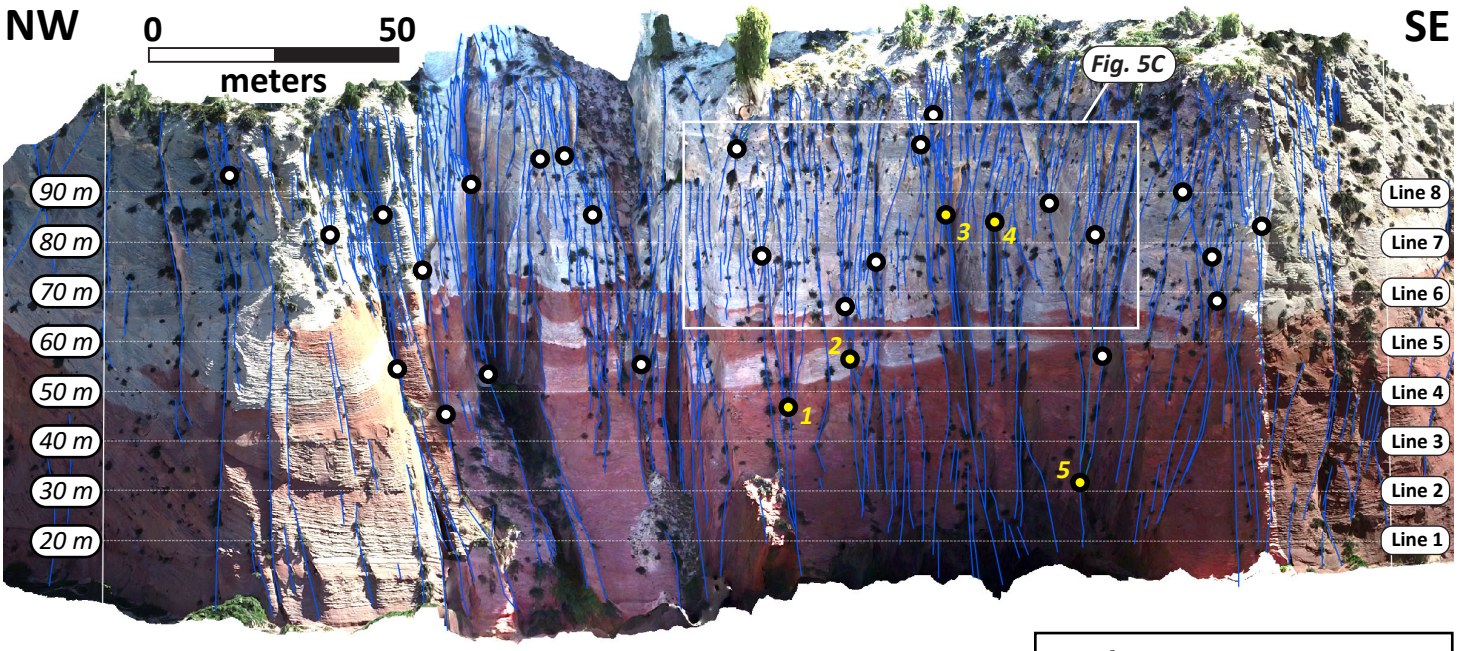

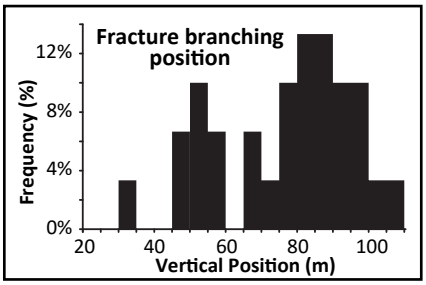

Figure 7. Orthomosaic image of VOM, displaying locations of each scanline and model-mapped fractures (blue lines). Image (from VOM) projected onto vertical plane oriented N30°W (see Fig. 6). VOM-based scanlines are spaced at 10-m intervals, with Line 1 at approximately 20 m elevation above the ground-based field scanline. All scanlines are 260 m in length. White dots indicate prominent fracture branching initiation points, and yellow dots indicate branching geometries documented in Fig. 8. Histogram (right) displays vertical distribution of branching initiation points. White box outlines area displayed in Figure 5C. Image altered to brighten the central region, which was in shadow at the time of UAV image capture.

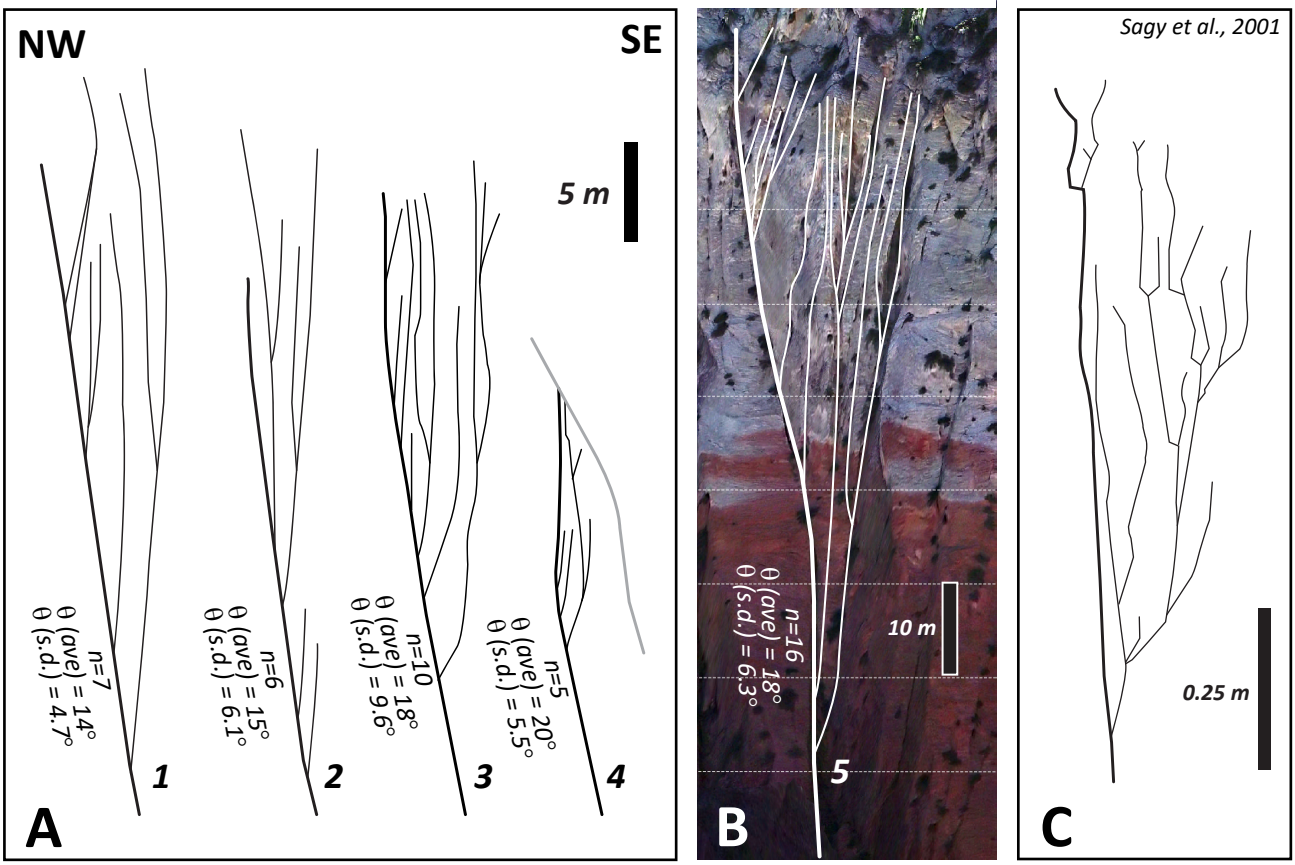

Figure 8. Representative "tree-like" fracture branching geometries along steeply dipping fractures (location of each branching geometry indicated on Fig. 7). Beside each geometry, we include the number of branch junctions (n) as well as the average and standard deviation for all branch angles. **A.** displays four examples of branching geometries traced from photos or VOM. In these diagrams, the initial primary fracture is bold and the bold gray line in 4 represents is a fracture against which two fractures terminate. The upward extents of most fractures in 1 - 3 cannot be traced higher due to poor exposure near the top of the study outcrop. **B.** dipslays branching geometry that extends from near the base of the outcrop to the top of the exposure (~80 meters vertical exposure). **C.** displays representative tree-like branching geometry of Sagy et al. (2001) (modified from Fig. 4a *in* Sagy et al., 2001).

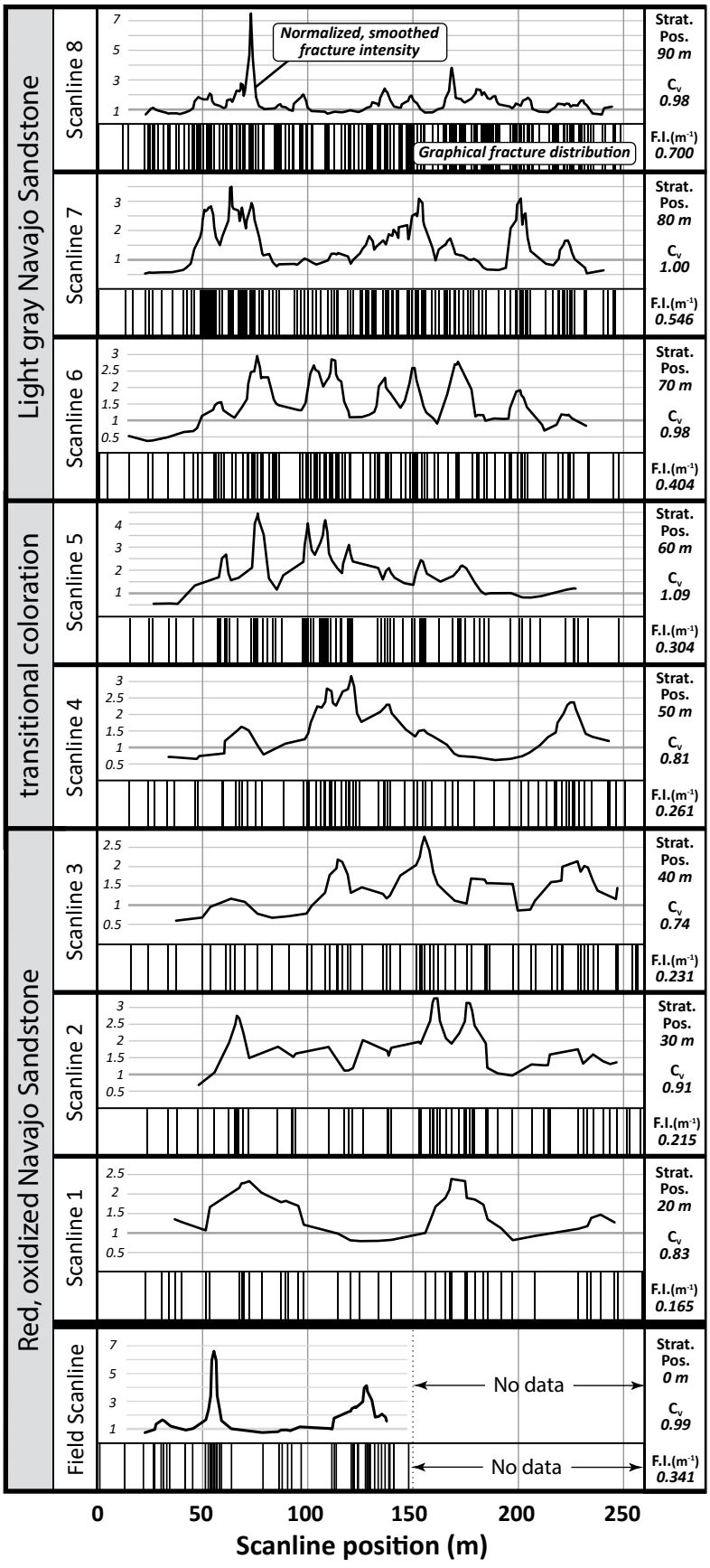

Figure 9. Scanline data from 9 stratigraphic levels, measured relative to the approximate base of the VOM in Red Hollow Canyon. Field-based coloration of the Jurassic Navajo sandstone is displayed on the left. Graphical fracture distributions are displayed at the bottom of each scanline box, and normalized fracture intensities are shown above each fracture distribution. Values were smoothed across 5-fracture populations then normalized relative to that scanline's average fracture intensity. A value of 1 on each graph represents the average fracture intensity value shown to the right. Fracture data are summarized in Table 1. Data from ground-based observations are displayed at the bottom, with VOM-derived scanlines 1-8 shown with increasing elevation.

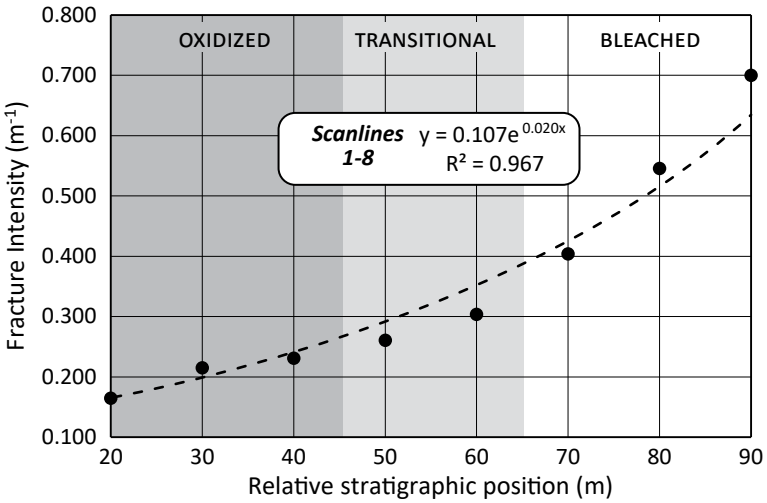

Figure 10. Changes in fracture intensity with stratigraphic position. Scanlines 1-3 are from the red, oxidized zone, scanlines 4 and 5 are from the transitional zone, and scanlines 6-8 are from the bleached zone of the Navajo Sandstone (Fig. 7). All VOM-based scanline data suggest a strong exponential relationship between stratigraphic position and fracture intensity (R^2=0.967).

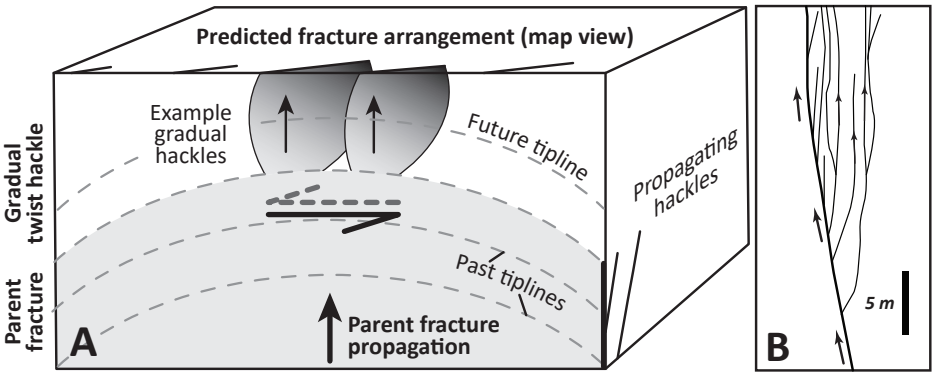

Figure 11. Proposed model for natural fracture branching in the Jurassic Navajo Sandstone. **A.** Generalized diagram of gradual twist-hackle formation during upward propagation of the parent fracture in a mixed-mode I-III loading configuration (see Mode III loading arrows). Front face of block diagram represents the parent fracture plane. Although parent fracture tipline instability leads to twist hackle initiation, we suggest that the parent fracture continued to propagate upward in concert with upward and lateral hackle propagation and the intitaion of new twist hackle at higher stratigraphic levels. Figure significantly modified from Youens and Engelder (1999) and Pollard et al. (1982). **B.** Diagram of branched fracture complex "3" on Fig. 8A, which represents the finite geometry of the system. The bold line represents the parent fracture. We suggest the non-terminating upward parent fracture propagation prohibits any significant lateral hackle propagation across the parent fracture plane.

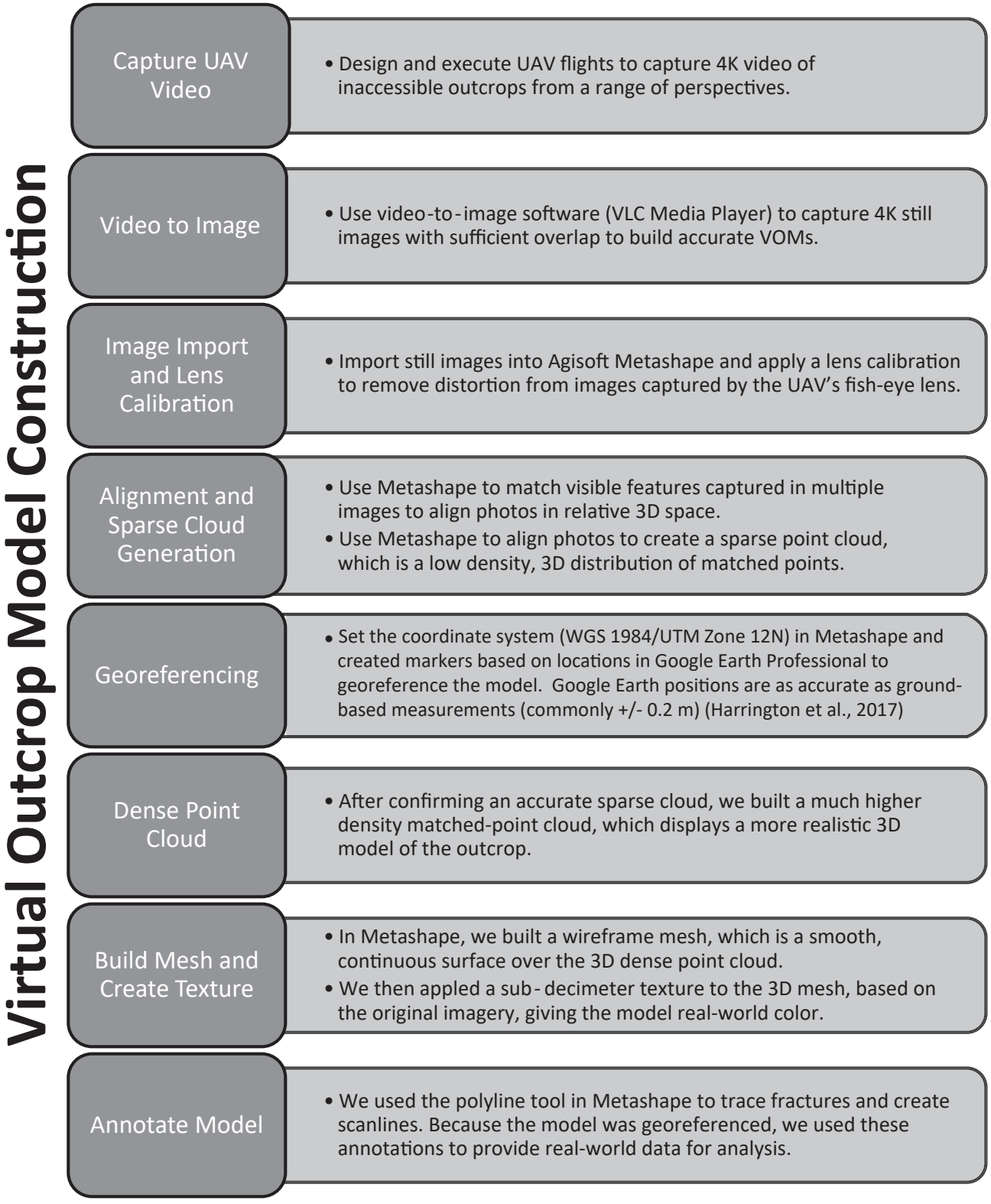

Figure A. Graphic Virtual Outcrop Model construction workflow, from UAV-based image capture to 3D model annotation. We primarily used the Agisoft Metashape Professional User Manual (v. 1.6) to develop this workflow. Please refer to that publication (Agisoft Metashape, 2020) for details.